InSAR Svalbard Ground Motion Service: Product Description and User Manual

Authors

Marie Bredal[1], Line Rouyet[2], Lotte Wendt[2], Heidi Hindberg[2], Daniel Stødle[2], Tom Rune Lauknes[2], Jelte van Oostveen[2], Yngvar Larsen[2], Gökhan Aslan[1], Emma Hauglin[1], John Dehls[1], Anja Sundal[3,4], Anna Odh[3], Dag Anders Moldestad[3]

[1] Geological Survey of Norway, Trondheim, 7040, Norway
[2] NORCE Research AS, Tromsø, 9294, Norway
[3] Norwegian Space Agency (NOSA), Oslo, 0277, Norway
[4] University of Oslo (UiO), Oslo, 0316, Norway

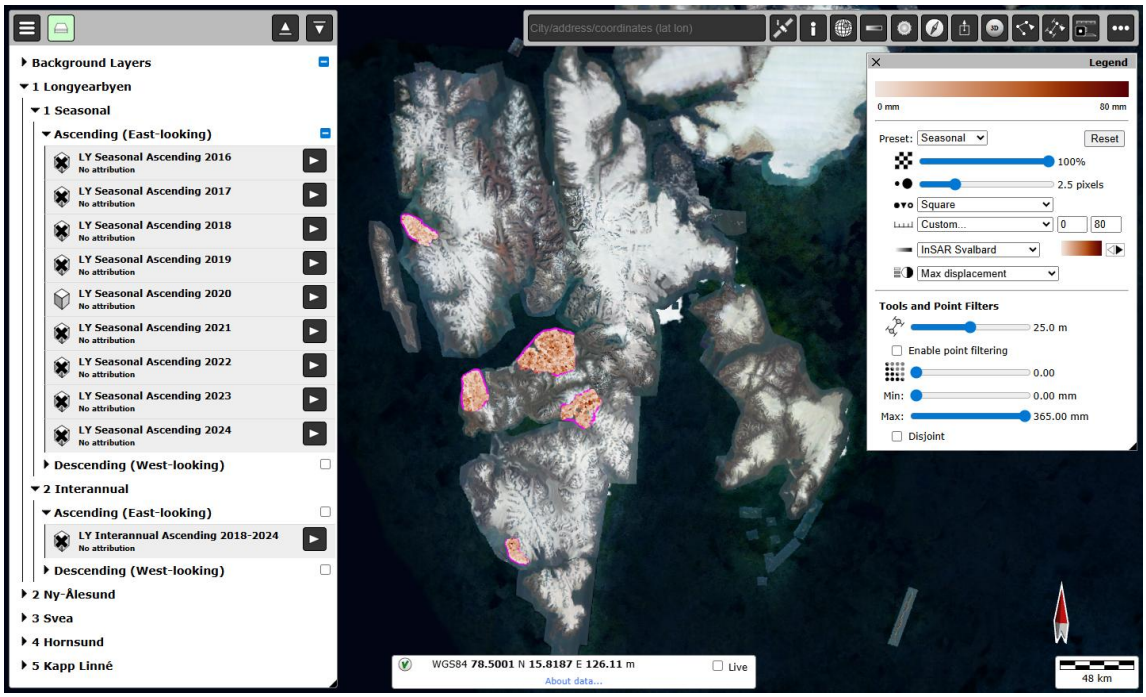

Date: 12.05.2026

Online service:

InSAR Svalbard Ground Motion Service: svalbard.insar.no

Summary

InSAR Svalbard is a partnership between the Geological Survey of Norway (NGU), NORCE Research AS and the Norwegian Space Agency (NOSA). The project aims to develop a Ground Motion Service (GMS) in Svalbard, providing spaceborne Synthetic Aperture Radar Interferometry (InSAR) ground displacement maps and time series tailored to Arctic conditions.

This report presents the data properties and WebGIS functions of the first open release of the InSAR Svalbard GMS. The service is openly available at svalbard.insar.no (release date: 02 February 2026). The pilot products are also distributed in the Zenodo data repository (Bredal et al., 2026; doi.org/10.5281/zenodo.18442696). This document is a user manual that introduces the processing method, describes the product properties and provides guidance on how to analyse and interpret the results in the web-based visualisation tool.

Acknowledgment

The InSAR Svalbard development project (2023–2025) included many rounds of interactions between InSAR experts and end-users throughout its design and implementation phases. Several user workshops and surveys were organised to define the product specifications, gather feedback on the first results and discussed the adjusted versions.

We acknowledge the involvement of key institutions and local stakeholders in Svalbard, which help defining the user requirements. We are especially grateful to the representatives from the Governor of Svalbard, the Longyearbyen Community Council, Store Norske Spitsbergen Kulkompani, Avinor, the Norwegian Polar Institute, the Norwegian Meteorological Institute, the University Centre in Svalbard, the Norwegian Geotechnical Institute and SINTEF AS.

We acknowledge all participants of the three InSAR Svalbard workshops (summer 2023, fall 2024 and fall 2025) for their questions and feedback, which contributed to improve the product specifications and the service functionalities (in alphabetic order): ANGELL Elisabeth, BARTSCH Annett, BØRVE HERNES Jostein, CHRISTIANSEN Hanne H., DUDEK Justyna, DUPUIS Sonia, FOTHERINGHAM Morag, FRAUENFELDER Regula, HARCOURT, William, HAARPAINTNER Jörg, INSTANES Arne, ISAKSEN Ketil, JAWAK Shridhar, JOCHMANN Malte, KRISTENSEN Lene, KÄÄB Andreas, LEFEUVRE Pierre-Marie, LEYDIER Matthieu, LONAR Vigdis, MARKUSSON Eystein, MOHOLDT Geir, MORRIS Ashley, NILSSEN Mariann, OLSEN INGERO Kjersti, PETER Maria, RAVOLAINEN Virve, RISVAAG Lillian, RUBENSDOTTER Lena, SCHELLENBERGER Thomas, SCHYTT MANNERFELT Erik, SERAFINSKA Monika, SINITSYN Anatoly, SKEDSMO Martin, THOMAS MITHAN Huw, THUESTAD Alma, VERRET Marjolaine, VICKERS Hannah, WEERDESTEIJN Maaike, WESTERMANN Sebastian, WILLMES Clarissa, ZHENG Duan.

Funding

The InSAR Svalbard Development Project (2023–2025) has been funded by the Norwegian Space Agency (NOSA) (Post 74, contract 74CO2301) and the Geological Survey of Norway (NGU). Recent research on InSAR in Svalbard and its use for permafrost science and geohazard assessment have also been supported by the ESA CCI Permafrost project (4000123681/18/I-NB) and the Fram Centre PermaRICH project (Ministry of Climate and Environment, chap. 1747, post 70).

Table of Contents

1. Introduction 3

1.1. Background and relevance 3

1.2. Project timeline 4

2. Interferometric Synthetic Aperture Radar (InSAR) 6

2.1. InSAR basics and measurement geometry 6

2.2. Small Baseline Subset (SBAS) processing 8

3. InSAR Svalbard products 11

3.1. Study areas 11

3.2. Products overview 12

3.3. Data format 18

4. InSAR Svalbard WebGIS tool 20

4.1. General WebGIS layout 20

4.2. WebGIS navigation 22

4.3. Background layers 23

4.4. Map viewer 24

4.5. Time series viewer 27

4.6. Data sharing and download 32

5. InSAR Svalbard data interpretation 33

5.1. Limitations and uncertainties 33

5.2. Spatial interpretation of InSAR Svalbard maps 35

5.3. Temporal interpretation of InSAR Svalbard time series 37

6. References 39

1. Introduction

1.1. Background and relevance

Svalbard is a dynamic High Arctic environment where diverse natural processes and human activities continuously shape the landscape and influence ground stability. Approximately 60% of the archipelago is covered by glaciers, while most of the remaining terrain is underlain by permafrost beneath an active layer that freezes and thaws seasonally (Hanssen-Bauer et al., 2019). The contrasting topography of the archipelago leads to a complex combination of periglacial processes, both in permafrost lowlands and mountain slopes. The diverse environmental and climatic conditions result in ground surface movement that varies in both amplitude and timing, reflecting the interplay of various geomorphic processes across the landscape (Rouyet et al., 2019).

The Arctic is warming three to four times faster than the global average. Svalbard is among the fastest-warming Arctic regions, with temperatures increasing up to seven times faster than the global average (AMAP, 2021; Rantanen et al., 2022). Consequently, permafrost temperature and active layer thickness are also increasing, both globally (Biskaborn et al., 2019) and in Svalbard (Strand and Christiansen, 2025). Such rapid warming leads to major environmental changes and increased ground dynamics. Permafrost degradation results in surface subsidence due to ground ice melting (O'Neill et al., 2023; Streletskiy et al., 2025). It also contributes to increasing the frequency, magnitude, and speed of landslides and other slope processes (Harris et al., 2011; Swanson, 2021).

Svalbard hosts a rich cultural heritage and diverse present-day human activities (Middleton, 2023). Unstable ground conditions pose a threat to historical sites (Nicu et al., 2025), modern infrastructure and human activities at the main settlements, research stations and tourist destinations (Hjort et al., 2022). Ground dynamics from changing ground thermal conditions can also alter the mobilisation and distribution of contaminants from identified polluted sites in Svalbard (Granberg et al., 2017). Mapping surface displacement is therefore highly relevant for geohazard assessment and management. In addition, Svalbard is a key location for many polar and climate science disciplines due to its unique environmental and climatic setting. Because the ground dynamics respond to environmental drivers, systematically measured surface displacement time series could be used as climate change indicators (Duchossois et al., 2018).

Spaceborne Interferometric Synthetic Aperture Radar (InSAR) is a remote sensing technique widely used to measure ground motion resulting from both natural (e.g., landslides, earthquakes, volcanoes) and anthropogenic (e.g., urban subsidence, building deformation, mining) processes (Rosen et al., 2002). InSAR is particularly valuable in remote and harsh environments such as permafrost terrain in polar regions and high mountains, where field-based observations are difficult and expensive to obtain (Zwieback et al., 2024). The Copernicus Sentinel-1 satellite mission, launched in 2014, acquires C-band radar images with a global coverage, a consistent acquisition strategy, and a short revisit time (6–12 days) (Geudtner et al., 2014). Its open data policy enables the development of operational InSAR Ground Motion Services (GMS) for large-scale surface displacement monitoring. On the Norwegian mainland, the InSAR Norway mapping service has provided nationwide, open-access InSAR data since 2018 (insar.ngu.no; Dehls et al., 2019). At the continental scale, the European Ground Motion Service (EGMS) provides similar products (egms.land.copernicus.eu; Costantini et al., 2021). Neither service currently includes the Svalbard archipelago.

Previous InSAR studies in Svalbard have demonstrated the potential of InSAR for mapping geohazards (Rouyet et al., 2017), inferring sediment frost-susceptibility (Rouyet et al., 2019) and ground ice content (Wendt et al., 2026), and documenting seasonal freeze–thaw cycles with subsidence–heave time series (Rouyet et al., 2021). Similar studies in other permafrost regions confirm the increasing use of InSAR for both geohazard management and permafrost research (e.g., Daout et al., 2017; Strozzi et al., 2018; Zwieback and Meyer, 2021; Wang et al., 2020). Most previous studies have been limited to small areas, short time periods and targeted applications, resulting in scattered datasets both in space and time. A consistently processed, open-access InSAR GMS has so far been lacking in the Arctic. The InSAR Svalbard GMS aims to fill this gap by providing displacement products for both research and operational use.

1.2. Project timeline

The InSAR Svalbard development project started in 2023 and included several rounds of interaction between InSAR experts and end-users throughout its design and implementation phases. User involvement has been essential to ensuring the relevance and applicability of the final products.

In 2023, we focused on defining the product specifications in dialogue with a reference group composed of representatives from governmental and private institutions in Svalbard, as well as remote sensing experts and polar research scientists. A first user workshop was held in Longyearbyen in summer 2023, to initiate the dialogue with key stakeholders. The Governor of Svalbard, the Longyearbyen Community Council, Store Norske Spitsbergen Kulkompani, Avinor, the Norwegian Polar Institute, the Norwegian Meteorological Institute, the University Centre in Svalbard, the Norwegian Geotechnical Institute and SINTEF AS were represented. We had valuable discussions on the planned features of the service, the relevant applications of InSAR data, and the potential synergies with other ongoing initiatives. An online survey was carried out in parallel to expand on the workshop findings and account for a wider range of user perspectives. The survey gathered inputs on current and planned uses of InSAR data, preferred GMS features and user requirements in terms of format, data coverage, resolution and update frequency. The responses confirmed a strong interest in developing an operational, dependable and user-friendly GMS tailored to Arctic conditions. The InSAR Svalbard report on the user requirements, technical considerations and product development plan summarised the conclusions drawn from both the workshop and the survey (hdl.handle.net/11250/3125660; Rouyet et al., 2024).

In 2024, we developed the first versions of the pilot products and the visualisation solution, with a focus on two priority areas (Longyearbyen and Ny-Ålesund). In fall 2024, a second dedicated user workshop was held in Oslo. The users had received access to the products beforehand. Feedback was gathered during the workshop and through an online user survey. The comments reflected the users' experience with the pilot products and the web-based 3D visualisation tool, highlighting both the strengths and potential for improvement. The feedback provided several suggestions for product refinement, improved documentation, extended spatial coverage and enhanced WebGIS functionalities.

In 2025, we refined the processing strategy and visualisation tool to better meet the user needs. We reprocessed the initial areas and extended the production to three new areas (Svea, Hornsund and Kapp Linné) for the first open release of the InSAR Svalbard GMS. A final workshop was held in Oslo in October 2025, and the launch day was organised in Longyearbyen in February 2026. As a result

of this iterative co-production phase, the first release of the InSAR Svalbard GMS is closely aligned with the user requirements of its target reference group.

The current document describes the data and service properties of the first open release of the InSAR Svalbard GMS. The project is planned to continue in the future, to refine the products, update the results with new seasons and gradually expand the coverage.

2. Interferometric Synthetic Aperture Radar (InSAR)

This chapter gives a brief summary of the theoretical background necessary to understand the InSAR Svalbard products. It is not meant to give a complete InSAR overview. For readers who want to learn more about the method, please read the InSAR Norway user guide on the NGU website (NGU, 2026) or refer to traditional InSAR literature (e.g., Bamler & Hartl, 1998; Massonnet & Feigl, 1998; Rosen et al., 2002; Hanssen, 2001; Woodhouse, 2006; Ferretti, 2014). For past InSAR research in Svalbard, and specific challenges related to the Arctic conditions, please refer to the first InSAR Svalbard report (hdl.handle.net/11250/3125660; Rouyet et al., 2024).

2.1. InSAR basics and measurement geometry

InSAR Svalbard results are based on C-band Synthetic Aperture Radar (SAR) images acquired by the Copernicus Sentinel-1 satellites, operating at a wavelength of ~5.6 cm. Interferometric SAR (InSAR) uses the phase of the radar signal, which is proportional to the two-way travel path between the satellite sensor and the ground surface. By comparing the phase of two satellite images acquired at different times over the same area, it is possible to measure changes in the sensor-to-ground distance along the radar line-of-sight (LOS). Such phase differences are represented as interferograms. Cumulative displacement time series can be derived by combining multiple interferograms.

InSAR is best suited for detecting slow, spatially coherent deformation. When surface changes occur too rapidly, or when the scattering properties vary significantly between acquisitions, the interferometric coherence decreases, and the phase information becomes unreliable. Such decorrelated areas must be discarded. The maximum unambiguous displacement measurable between two acquisitions is half the radar wavelength (~2.8 cm for Sentinel-1). Larger displacements result in phase wrapping, introducing ambiguity in the measured phase. Successful phase unwrapping requires spatially smooth phase gradients; if phase differences between neighbouring pixels exceed approximately a quarter wavelength (~1.4 cm), phase continuity may be lost, and unwrapping errors can occur. Consequently, areas with high deformation rates (decimetre to metre-scale per year) are often not reliably captured, even when using image pairs with a short time interval (e.g., 6 days for Sentinel-1).

SAR satellites operate with a side-looking geometry, and InSAR measurements are inherently one-dimensional, capturing displacement along the LOS (**Figure 1**, A). As such, InSAR does not provide full three-dimensional displacement vectors, but only the movement component projected onto the viewing direction (LOS). The LOS geometry is defined by the incidence angle (angle between the radar beam and the normal to the surface), the track angle (flight direction) and the azimuth angle (compass direction of the LOS, perpendicular to the flight direction) (**Figure 1**, B). The track and azimuth angles vary depending on the orbit configuration. Sentinel-1 acquires data in both ascending (south-to-north) and descending (north-to-south) orbits, resulting in different viewing geometries (**Figure 1**, C).

Due to the near-polar orbit and the side-looking geometry, InSAR is generally more sensitive to east-west and vertical motion than to north-south displacement. The sign of the displacement value indicates the movement direction relative to the satellite position: positive values correspond to movement toward the sensor, and negative values to movement away from the sensor. For example, if a landform is creeping downslope toward the west, the ground is moving toward the

sensor in an ascending orbit (positive values) and away from the sensor in a descending orbit (negative values) (**Figure 2**).

Topography strongly influences the radar measurements. Slopes facing the satellite may be affected by layover, while slopes oriented away from the sensor may be subject to radar shadow. Those geometric distortions prevent reliable phase measurements. Such areas are therefore masked out in the InSAR Svalbard products. Topographical, decorrelation and phase unwrapping limitations lead to spatially discontinuous data coverage. Data gaps in the InSAR Svalbard GMS maps do not imply an absence of deformation, but rather reflects areas where reliable InSAR measurements cannot be obtained due to inherent methodological and geometric constraints. Further details on these limitations are provided on the InSAR Norway website (NGU, 2026) and further discussed in **Section 5**.

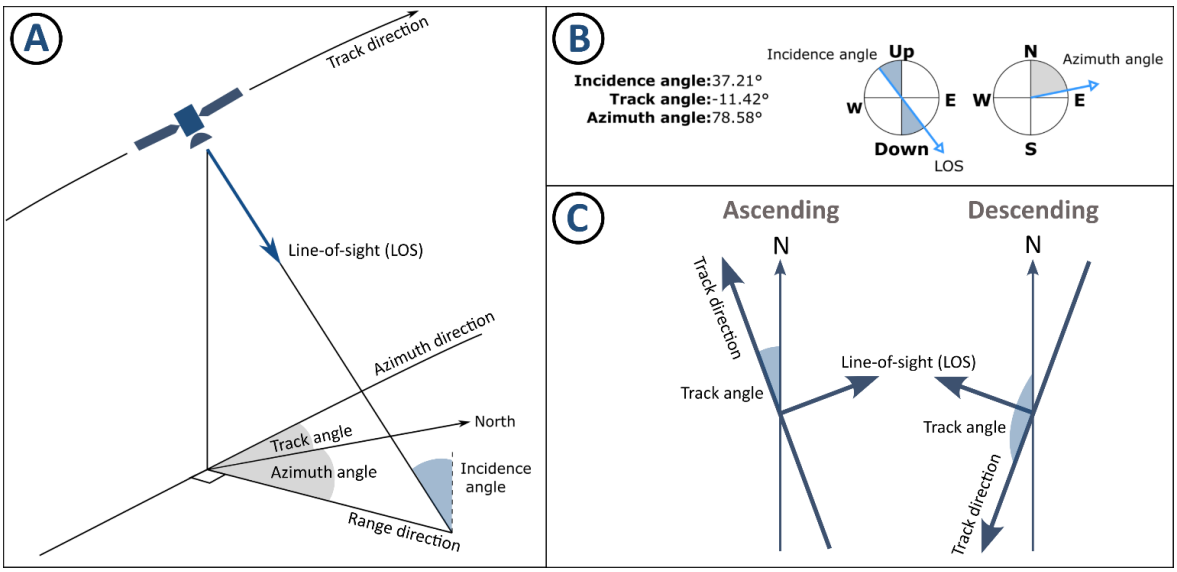

Figure 1. Schematic representation of the InSAR measurement geometry. **A.** Illustration of the SAR side-looking geometry highlighting the radar line-of-sight (LOS), depending on three key angles: the incidence, track and azimuth angles. **B.** Circular plots used in the InSAR Svalbard WebGIS to document the key angles determining the radar LOS. **C.** Schematic map representation of the ascending and descending orbits and resulting track angles and LOS for both geometries (modified from NGU, 2026).

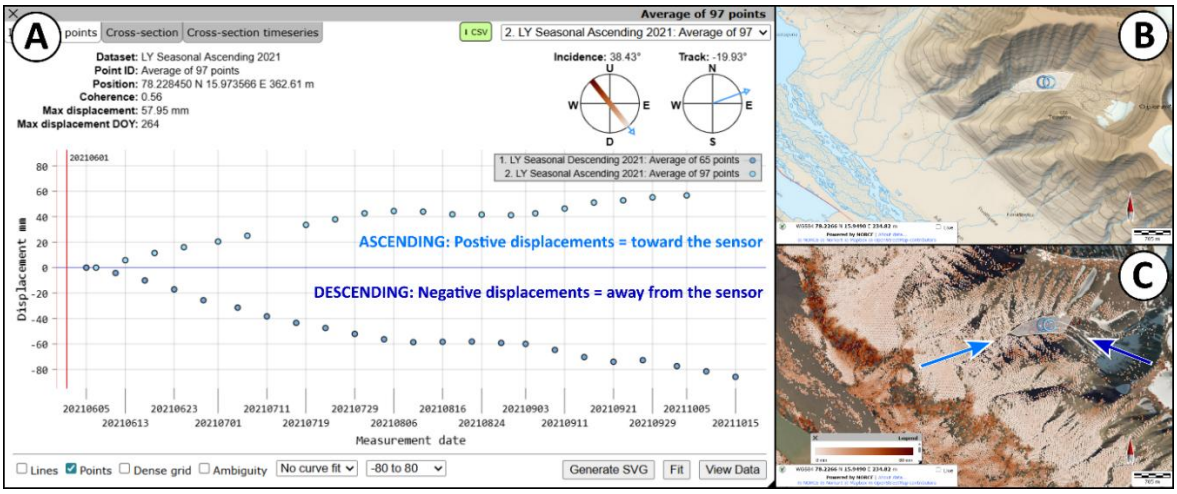

Figure 2. Effect of the SAR viewing geometry on the detected InSAR displacement. **A.** Displacement time series from an average of pixels over a rock glacier in Ugledalen, Central Spitsbergen. The time series shows positive LOS displacement values in the ascending geometry (light blue) and negative displacement values in the descending geometry (dark blue). **B.** Location map of the white shaded polygon used for averaging. The rock glacier moves downslope towards the west. Background: Svalbard Topography (NPI, 2026a). **C.** The rock glacier moves toward the sensor in an ascending orbit (LOS: light blue arrow). The same landform moves away from the sensor in a descending orbit (LOS: dark blue arrow). Background: Svalbard Orthophoto (NPI, 2026b).

2.2. Small Baseline Subset (SBAS) processing

The InSAR Svalbard products were generated using a Distributed Scatterer InSAR approach, based on the SBAS algorithm (Berardino et al., 2002), implemented in the NORCE SAR processing software (Larsen et al., 2006). The SBAS approach uses a network of interferograms selected according to predefined spatial and temporal baseline thresholds to minimize geometric and temporal decorrelation. By combining multiple, partially overlapping interferograms, the method increases redundancy, reduces atmospheric noise, and improves the accuracy of the displacement estimates (Lauknes et al., 2010). Precise orbits and a 20 m Digital Elevation Model (DEM) from the Norwegian Polar Institute (NPI, 2014) were used to remove orbital and topographic phase components, and phase unwrapping was performed using a minimum-cost flow algorithm (Chen and Zebker, 2002). The processing workflow followed the same steps applied to past Svalbard case studies (Rouyet et al., 2019; 2021; Wendt et al., 2026). Details regarding the processed areas, LOS geometries, reference locations for calibration, time periods, numbers of interferograms and documented pixels after filtering are summarised in **Tables 1–6**. Limitations and uncertainties related to the processing are further discussed in **Section 5.1**.

We used Sentinel-1 SAR images acquired in the Interferometric Wide (IW) swath mode from track 14A (ascending geometry) and track 154D (descending geometry). For each year, only images from the snow-free seasons were processed, because snow causes decorrelation of the phase signal. The observation time window varies each year due to variable climatic conditions. At best, the documented period extends from late May to early December.

To improve the signal stability, a spatial multi-looking factor of 8×2 (range × azimuth) was applied to the IW images, resulting in a final ground resolution of ~30 m. The temporal resolution

corresponds to the satellite's revisit interval: 6 days during dual-satellite operation (2017–2021); 12 days before fall 2016 and after the Sentinel-1B failure in December 2021.

Two complementary SBAS processing strategies were applied to generate two different types of InSAR Svalbard GMS products, capturing both short-term (seasonal) and long-term (interannual) ground surface displacement patterns. This dual processing approach enables InSAR Svalbard products to capture ground dynamics across multiple timescales.

1) Seasonal products

The seasonal products document cumulative, short-term surface displacement within each snow-free period. The time series span 2016–2024 for ascending products and 2018–2024 for descending products. In three areas, 2024 results were discarded in ascending geometry due to insufficient exploitable data after discarding interferograms affected by strong decorrelation and major ionospheric and atmospheric effects.

Interferograms were generated using image pairs with short temporal baselines (6–48 days). Each season was processed separately. As a result, each seasonal time series starts at 0 mm. Potential movement occurring before the start date is not captured and any ongoing long-term trends are not reflected in these results.

The time series are used to extract the maximum seasonal displacement in mm (attribute "maxdisp") and the timing of this maximum displacement, expressed as Day of Year (DOY) (attribute "doymax"). The products enable the documentation of seasonal patterns and fast-moving areas (up to a couple of decimetres within one snow-free season). The seasonal products are well suited for identifying rapid surface changes that occur within a single snow-free season, such as active layer dynamics or slope movement.

2) Interannual products

The interannual products document cumulative, long-term surface displacement occurring between consecutive snow-free periods. The time series span 2018–2024, both for ascending and descending products, to provide an easily comparable period.

Interferograms were generated using image pairs separated by approximately one year (340–390 days of temporal baselines), using July to September images. Areas that experience large changes during the winter are affected by phase decorrelation at the interannual scale. Fewer pixels are therefore documented on slopes and fast-moving landforms. However, areas with late-lying snow, potentially discarded in the seasonal products, might be better covered by the interannual products due to the focus on late summer and fall images only. These products are not intended to document seasonal patterns.

The time series are used to estimate the interannual mean velocity along the LOS in mm/yr (attribute "trend"). The products enable the documentation of slow, gradual displacement patterns over multiple years (up to a couple of centimetres per year), e.g., due to subsidence from permafrost degradation, heave from ice aggradation, or downslope movement from permafrost creep.

Various filtering techniques have been applied to discard low-quality pixels, irrelevant signals and areas likely to be affected by unwrapping errors and phase ambiguities:

- **Signal stability filter**: For seasonal products, we removed pixels with an overall mean coherence < 0.45. For discarding areas with low coherence at the beginning of the season,

where there are late-lying snow or wet surfaces, we applied an additional filter based on coherence time series. The pixels were discarded where the averaged coherence was < 0.45 during the first four acquisitions of the seasons (for years with 6-days temporal resolution) or the first two acquisitions of the seasons (for years with 12-days temporal resolution). For interannual products, we removed pixels with an overall mean coherence < 0.35. No other coherence time series filter has been applied for interannual products, considering that these products are based on late summer and fall images only.

- **Phase ambiguity filter**: The pixels affected by large displacement gradients in time were discarded. For seasonal products, we applied a conservative threshold of a quarter of the radar wavelength (> 1.4 cm) between consecutive acquisitions to identify and remove pixels likely to be affected by decorrelation, phase ambiguities and unwrapping errors. For interannual products, we applied a more liberal threshold of half a wavelength (> 2.8 cm) due to longer time spans. With such a filter, areas affected by major decorrelation and unwrapping errors are likely discarded but the users must still treat carefully pixels moving > 1.4 cm/year, as those might be affected by phase ambiguities.
- **DEM-error filter**: For both seasonal and interannual products, we removed pixels with SBAS-estimated DEM-corrections exceeding ± 20 m, compared to the applied external DEM (NPI, 2014).

The choice of filtering settings represents a challenging trade-off. We aim to avoid the inclusion of uncertain and potentially biased information while preserving the most interesting areas. These settings are still under evaluation and may therefore evolve during the future development of the service.

3. InSAR Svalbard products

3.1. Study areas

InSAR Svalbard seasonal and interannual products are available for five study areas: Longyearbyen (LY), Ny-Ålesund (NY), Kapp Linné (KL), Svea (SV) and Hornsund (HS). The geographic locations and extents of these study areas are shown in **Figure 3**. These areas were selected due to their societal and scientific relevance, as they include main Norwegian settlements, research stations, tourist destinations and cultural heritage sites (Rouyet et al., 2024)**.** Details of each available product are provided in **Sections 3.2–3.3**.

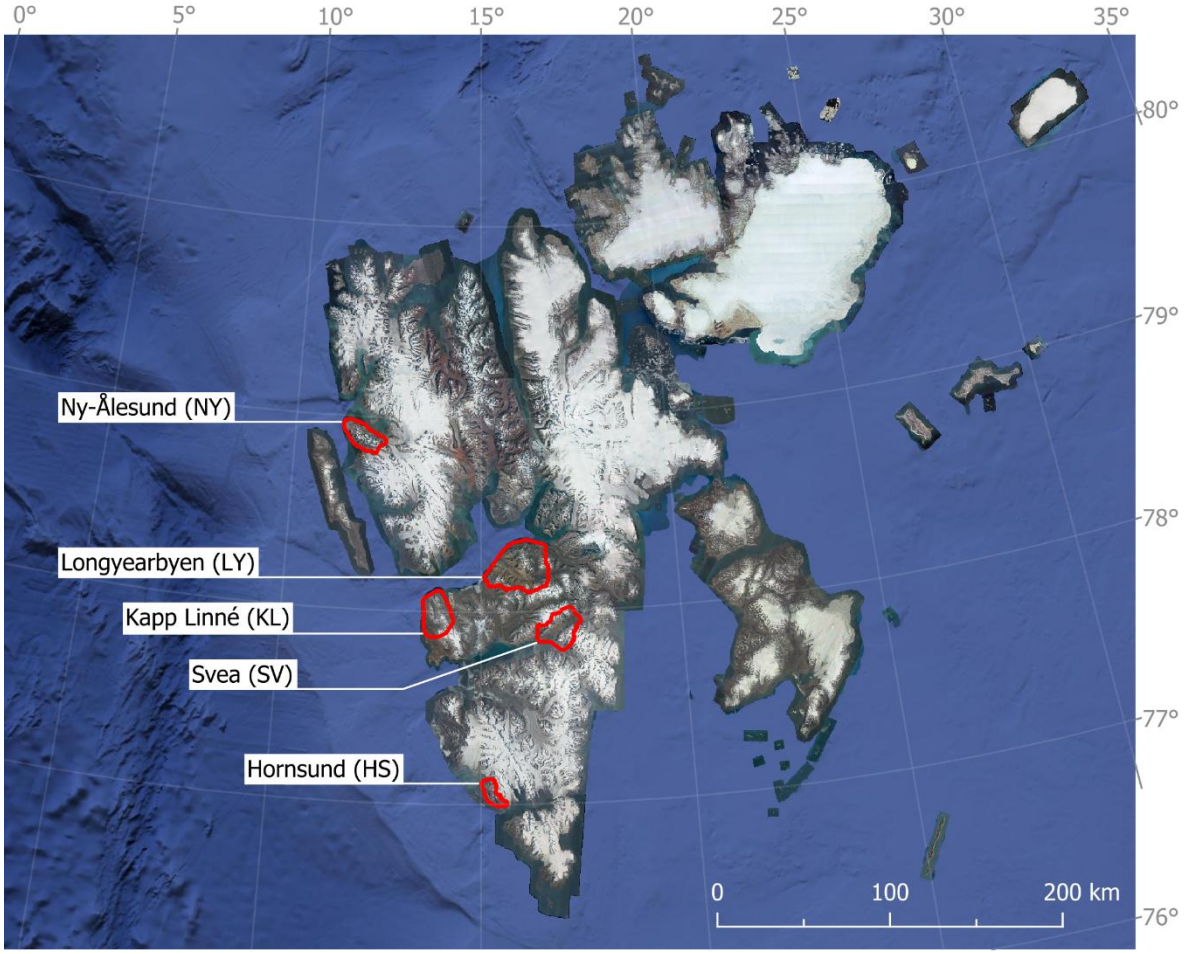

Figure 3. Overview of the five study areas with available InSAR Svalbard products: Longyearbyen (LY), Ny-Ålesund (NY), Svea (SV), Hornsund (HS) and Kapp Linné (KL). Background: Svalbard Orthophoto (NPI, 2026b) and Google Satellite Orthoimages.

3.2. Products overview

Table 1 gives an overview of the main properties of each study area. The properties of all available InSAR Svalbard pilot products are summarised in **Tables 2–6**, grouped by study area: Longyearbyen (**Table 2**), Ny-Ålesund (**Table 3**), Svea (**Table 4**), Hornsund (**Table 5**) and Kapp Linné (**Table 6**).

The spatial resolution is consistent across all products (~30 m). The temporal resolution depends on satellite availability, with 6-day intervals during periods when both Sentinel-1A and Sentinel-1B were operational (Fall 2016–2021), and 12-day intervals when only one satellite was available (Spring–Fall 2016 and 2022–2024).

Tables 2–6 include the dataset name in the WebGIS interface (svalbard.insar.no) and the Zenodo data package (doi.org/10.5281/zenodo.18442696), the SAR geometry (ascending or descending), the product type (seasonal or interannual), the number of used interferograms (ifgs), the documented (doc.) pixels and the start/end dates, duration (days), number of acquisition (acqu.) dates of the time series.

Table 1. Area names, sizes, available products, line-of-sight track and incidence angles, and reference locations for calibration in the five InSAR Svalbard study areas. A = ascending orbit. D = descending orbit.

Study area name	Short name	Area size (km^2)	Seasonal products	Interannual Products	Line-of-sight track and incidence angles (°)	Reference location for calibration (°)
Longyearbyen	LY	811	A: 2016–2024 D: 2018–2024	A/D: 2018–2024	A track: -19.22 to -20.80 A incidence: 37.13 to 39.52 D track: -157.59 to -159.16 D incidence: 34.89 to 37.07	WGS84 Lat. 78.210236 WG684 Long. 15.613567
Ny-Ålesund	NY	264	A: 2016–2024 D: 2018–2024	A/D: 2018–2024	A track: -23.22 to -24.29 A incidence: 34.32 to 35.53 D track: -161.87 to -162.98 D incidence: 41.85 to 43.28	WGS84 Lat. 78.927330 WG684 Long. 11.931546
Svea	SV	379	A: 2016–2023* D: 2018-2024	A/D: 2018–2024	A track: -18.54 to -19.61 A incidence: 38.12 to 39.75 D track: -156.81 to -157.86 D incidence: 33.16 to 34.70	WGS84 Lat. 77.925323 WG684 Long. 16.857288
Hornsund	HS	123	A: 2016–2023* D: 2018-2024	A/D: 2018–2024	A track: -20.54 to -21.08 A incidence: 34.32 to 34.97 D track: -158.43 to -159.01 D incidence: 33.32 to 34.49	WGS84 Lat. 77.001259 WG684 Long. 15.391263
Kapp Linné	KL	359	A: 2016–2023* D: 2018–2024	A/D: 2018–2024	A track: -21.60 to -22.29 A incidence: 34.41 to 35.52 D track: -159.88 to -160.62 D incidence: 37.79 to 38.81	WGS84 Lat. 78.009750 WG684 Long. 13.686106

*The 2024 seasonal ascending product was discarded in three study areas (SV, HS and KL) due to low data quality.

Table 2. List of Longyearbyen (LY) products, available in the InSAR Svalbard WebGIS (underlined names) and the Zenodo data package (*italic names*). Start and end dates of the time series are shown in YYYYMMDD format (YYYY = year, MM = month, DD = day). Abbreviations: ifgs = interferograms, doc. = documented, acqu. = acquisition.

Dataset name in the WebGIS and *CSV data package*	**Product type**	**SAR geometry**	**Start date End date**	**Duration (days)**	**# acqu. dates**	**# used ifgs**	**# doc. pixels**
LY Seasonal Ascending 2016 *InSAR-Svalbard-LY-Seasonal-A-2016-v2026*	Seasonal	Ascending	20160703 20161130	150	19	49	253080
LY Seasonal Ascending 2017 *InSAR-Svalbard-LY-Seasonal-A-2017-v2026*	Seasonal	Ascending	20170610 20171119	162	28	96	262615
LY Seasonal Ascending 2018 *InSAR-Svalbard-LY-Seasonal-A-2018-v2026*	Seasonal	Ascending	20180605 20181126	174	30	82	250602
LY Seasonal Ascending 2019 *InSAR-Svalbard-LY-Seasonal-A-2019-v2026*	Seasonal	Ascending	20190618 20191127	162	27	78	287732
LY Seasonal Ascending 2020 *InSAR-Svalbard-LY-Seasonal-A-2020-v2026*	Seasonal	Ascending	20200525 20201109	168	28	86	319382
LY Seasonal Ascending 2021 *InSAR-Svalbard-LY-Seasonal-A-2021-v2026*	Seasonal	Ascending	20210607 20211005	120	20	79	283124
LY Seasonal Ascending 2022 *InSAR-Svalbard-LY-Seasonal-A-2022-v2026*	Seasonal	Ascending	20220602 20221012	132	12	24	279383
LY Seasonal Ascending 2023 *InSAR-Svalbard-LY-Seasonal-A-2023-v2026*	Seasonal	Ascending	20230609 20231007	120	10	13	147701
LY Seasonal Ascending 2024 *InSAR-Svalbard-LY-Seasonal-A-2024-v2026*	Seasonal	Ascending	20240603 20241001	120	11	15	184076
LY Seasonal Descending 2018 *InSAR-Svalbard-LY-Seasonal-D-2018-v2026*	Seasonal	Descending	20180603 20181112	162	28	81	191522
LY Seasonal Descending 2019 *InSAR-Svalbard-LY-Seasonal-D-2019-v2026*	Seasonal	Descending	20190622 20191125	156	27	74	300752
LY Seasonal Descending 2020 *InSAR-Svalbard-LY-Seasonal-D-2020-v2026*	Seasonal	Descending	20200529 20201107	162	28	84	333565
LY Seasonal Descending 2021 *InSAR-Svalbard-LY-Seasonal-D-2021-v2026*	Seasonal	Descending	20210605 20211015	132	23	85	245416
LY Seasonal Descending 2022 *InSAR-Svalbard-LY-Seasonal-D-2022-v2026*	Seasonal	Descending	20220531 20221010	132	12	23	200350
LY Seasonal Descending 2023 *InSAR-Svalbard-LY-Seasonal-D-2023-v2026*	Seasonal	Descending	20230607 20231017	132	12	15	146796
LY Seasonal Descending 2024 *InSAR-Svalbard-LY-Seasonal-D-2024-v2026*	Seasonal	Descending	20240601 20240929	120	11	16	171361
LY Interannual Ascending 2018–2024 *InSAR-Svalbard-LY-Interannual-A-2018-2024-v2026*	Interannual	Ascending	20180723 20240919	2250	52	135	340716
LY Interannual Descending 2018–2024 *InSAR-Svalbard-LY-Interannual-D-2018-2024-v2026*	Interannual	Descending	20180820 20240905	2208	50	146	300787

Table 3. List of Ny-Ålesund (NY) products, available in the InSAR Svalbard WebGIS (underlined names) and the Zenodo data package (*italic names*). Start and end dates of the time series are shown in YYYYMMDD format (YYYY = year, MM = month, DD = day). Abbreviations: ifgs = interferograms, doc. = documented, acqu. = acquisition.

Dataset name in the WebGIS and *CSV data package*	Product type	SAR geometry	Start date End date	Duration (days)	# acqu. dates	# used ifgs	# doc. pixels
NY Seasonal Ascending 2016 *InSAR-Svalbard-NY-Seasonal-A-2016-v2026*	Seasonal	Ascending	20160703 20161112	132	16	49	101253
NY Seasonal Ascending 2017 *InSAR-Svalbard-NY-Seasonal-A-2017-v2026*	Seasonal	Ascending	20170616 20171002	108	19	82	86631
NY Seasonal Ascending 2018 *InSAR-Svalbard-NY-Seasonal-A-2018-v2026*	Seasonal	Ascending	20180605 20180927	114	20	82	84312
NY Seasonal Ascending 2019 *InSAR-Svalbard-NY-Seasonal-A-2019-v2026*	Seasonal	Ascending	20190624 20191103	132	23	86	97542
NY Seasonal Ascending 2020 *InSAR-Svalbard-NY-Seasonal-A-2020-v2026*	Seasonal	Ascending	20200531 20201004	126	23	86	109416
NY Seasonal Ascending 2021 *InSAR-Svalbard-NY-Seasonal-A-2021-v2026*	Seasonal	Ascending	20210625 20211029	126	21	83	89816
NY Seasonal Ascending 2022 *InSAR-Svalbard-NY-Seasonal-A-2022-v2026*	Seasonal	Ascending	20220614 20221012	120	11	25	93682
NY Seasonal Ascending 2023 *InSAR-Svalbard-NY-Seasonal-A-2023-v2026*	Seasonal	Ascending	20230609 20230913	96	8	14	43957
NY Seasonal Ascending 2024 *InSAR-Svalbard-NY-Seasonal-A-2024-v2026*	Seasonal	Ascending	20240627 20241001	96	9	18	102655
NY Seasonal Descending 2018 *InSAR-Svalbard-NY-Seasonal-D-2018-v2026*	Seasonal	Descending	20180603 20180925	114	20	85	108224
NY Seasonal Descending 2019 *InSAR-Svalbard-NY-Seasonal-D-2019-v2026*	Seasonal	Descending	20190622 20191107	138	24	88	114873
NY Seasonal Descending 2020 *InSAR-Svalbard-NY-Seasonal-D-2020-v2026*	Seasonal	Descending	20200529 20201020	144	25	89	134571
NY Seasonal Descending 2021 *InSAR-Svalbard-NY-Seasonal-D-2021-v2026*	Seasonal	Descending	20210623 20211015	114	20	87	127356
NY Seasonal Descending 2022 *InSAR-Svalbard-NY-Seasonal-D-2022-v2026*	Seasonal	Descending	20220612 20221022	132	12	26	118081
NY Seasonal Descending 2023 *InSAR-Svalbard-NY-Seasonal-D-2023-v2026*	Seasonal	Descending	20230607 20230911	96	9	18	64015
NY Seasonal Descending 2024 *InSAR-Svalbard-NY-Seasonal-D-2024-v2026*	Seasonal	Descending	20240613 20240929	108	10	19	123349
NY Interannual Ascending 2018–2024 *InSAR-Svalbard-NY-Interannual-A-2018-2024-v2026*	Interannual	Ascending	20180711 20240919	2262	58	171	107898
NY Interannual Descending 2018–2024 *InSAR-Svalbard-NY-Interannual-D-2018-2024-v2026*	Interannual	Descending	20180715 20240824	2232	62	169	136782

Table 4. List of Svea (SV) products, available in the InSAR Svalbard WebGIS (underlined names) and the Zenodo data package (*italic names*). Start and end dates of the time series are shown in YYYYMMDD format (YYYY = year, MM = month, DD = day). Abbreviations: ifgs = interferograms, doc. = documented, acqu. = acquisition.

Dataset name in the WebGIS and *CSV data package*	Product type	SAR geometry	Start date End date	Duration (days)	# acqu. dates	# used ifgs	# doc. pixels
SV Seasonal Ascending 2016 *InSAR-Svalbard-SV-Seasonal-A-2016-v2026*	Seasonal	Ascending	20160703 20161124	144	18	43	105269
SV Seasonal Ascending 2017 *InSAR-Svalbard-SV-Seasonal-A-2017-v2026*	Seasonal	Ascending	20170616 20171107	144	25	80	139641
SV Seasonal Ascending 2018 *InSAR-Svalbard-SV-Seasonal-A-2018-v2026*	Seasonal	Ascending	20180605 20181021	138	24	69	88626
SV Seasonal Ascending 2019 *InSAR-Svalbard-SV-Seasonal-A-2019-v2026*	Seasonal	Ascending	20190618 20191127	162	28	78	118515
SV Seasonal Ascending 2020 *InSAR-Svalbard-SV-Seasonal-A-2020-v2026*	Seasonal	Ascending	20200531 20201028	150	26	93	112097
SV Seasonal Ascending 2021 *InSAR-Svalbard-SV-Seasonal-A-2021-v2026*	Seasonal	Ascending	20210619 20211011	114	19	82	116834
SV Seasonal Ascending 2022 *InSAR-Svalbard-SV-Seasonal-A-2022-v2026*	Seasonal	Ascending	20220602 20220930	120	11	21	109539
SV Seasonal Ascending 2023 *InSAR-Svalbard-SV-Seasonal-A-2023-v2026*	Seasonal	Ascending	20230621 20231007	108	9	13	107183
SV Seasonal Descending 2018 *InSAR-Svalbard-SV-Seasonal-D-2018-v2026*	Seasonal	Descending	20180603 20181019	138	24	67	65304
SV Seasonal Descending 2019 *InSAR-Svalbard-SV-Seasonal-D-2019-v2026*	Seasonal	Descending	20190622 20191125	156	25	71	101046
SV Seasonal Descending 2020 *InSAR-Svalbard-SV-Seasonal-D-2020-v2026*	Seasonal	Descending	20200529 20201026	150	26	78	103404
SV Seasonal Descending 2021 *InSAR-Svalbard-SV-Seasonal-D-2021-v2026*	Seasonal	Descending	20210611 20211003	114	20	82	86269
SV Seasonal Descending 2022 *InSAR-Svalbard-SV-Seasonal-D-2022-v2026*	Seasonal	Descending	20220531 20221010	132	12	19	79685
SV Seasonal Descending 2023 *InSAR-Svalbard-SV-Seasonal-D-2023-v2026*	Seasonal	Descending	20230619 20231017	120	11	14	73126
SV Seasonal Descending 2024 *InSAR-Svalbard-SV-Seasonal-D-2024-v2026*	Seasonal	Descending	20240613 20240927	106	9	11	66088
SV Interannual Ascending 2018–2024 *InSAR-Svalbard-SV-Interannual-A-2018-2024-v2026*	Interannual	Ascending	20180903 20240919	2208	28	64	99545
SV Interannual Descending 2018–2024 *InSAR-Svalbard-SV-Interannual-D-2018-2024-v2026*	Interannual	Descending	20180826 20240917	2214	35	67	69881

Table 5. List of Hornsund (HS) products, available in the InSAR Svalbard WebGIS (underlined names) and the Zenodo data package (*italic names*). Start and end dates of the time series are shown in YYYYMMDD format (YYYY = year, MM = month, DD = day). Abbreviations: ifgs = interferograms, doc. = documented, acqu. = acquisition.

Dataset name in the WebGIS and *CSV data package*	**Product type**	**SAR geometry**	**Start date End date**	**Duration (days)**	**# acqu. dates**	**# used ifgs**	**# doc. pixels**
HS Seasonal Ascending 2016 *InSAR-Svalbard-HS-Seasonal-A-2016-v2026*	Seasonal	Ascending	20160703 20161124	144	16	41	47729
HS Seasonal Ascending 2017 *InSAR-Svalbard-HS-Seasonal-A-2017-v2026*	Seasonal	Ascending	20170616 20171026	132	23	74	37605
HS Seasonal Ascending 2018 *InSAR-Svalbard-HS-Seasonal-A-2018-v2026*	Seasonal	Ascending	20180623 20181009	108	19	79	43944
HS Seasonal Ascending 2019 *InSAR-Svalbard-HS-Seasonal-A-2019-v2026*	Seasonal	Ascending	20190618 20191028	132	23	77	44849
HS Seasonal Ascending 2020 *InSAR-Svalbard-HS-Seasonal-A-2020-v2026*	Seasonal	Ascending	20200525 20201010	138	24	87	44329
HS Seasonal Ascending 2021 *InSAR-Svalbard-HS-Seasonal-A-2021-v2026*	Seasonal	Ascending	20210613 20211122	162	27	86	39868
HS Seasonal Ascending 2022 *InSAR-Svalbard-HS-Seasonal-A-2022-v2026*	Seasonal	Ascending	20220602 20220930	120	11	22	46831
HS Seasonal Ascending 2023 *InSAR-Svalbard-HS-Seasonal-A-2023-v2026*	Seasonal	Ascending	20230609 20230901	84	7	11	32961
HS Seasonal Descending 2018 *InSAR-Svalbard-HS-Seasonal-D-2018-v2026*	Seasonal	Descending	20180621 20181007	108	19	74	47467
HS Seasonal Descending 2019 *InSAR-Svalbard-HS-Seasonal-D-2019-v2026*	Seasonal	Descending	20190616 20191107	144	24	85	51183
HS Seasonal Descending 2020 *InSAR-Svalbard-HS-Seasonal-D-2020-v2026*	Seasonal	Descending	20200529 20201008	132	23	83	55709
HS Seasonal Descending 2021 *InSAR-Svalbard-HS-Seasonal-D-2021-v2026*	Seasonal	Descending	20210611 20211015	126	22	76	47173
HS Seasonal Descending 2022 *InSAR-Svalbard-HS-Seasonal-D-2022-v2026*	Seasonal	Descending	20220531 20221010	132	12	20	50269
HS Seasonal Descending 2023 *InSAR-Svalbard-HS-Seasonal-D-2023-v2026*	Seasonal	Descending	20230607 20230830	84	8	11	37180
HS Seasonal Descending 2024 *InSAR-Svalbard-HS-Seasonal-D-2024-v2026*	Seasonal	Descending	20240707 20240929	84	8	11	53018
HS Interannual Ascending 2018–2024 *InSAR-Svalbard-HS-Interannual-A-2018-2024-v2026*	Interannual	Ascending	20180723 20240919	2250	62	178	53173
HS Interannual Descending 2018–2024 *InSAR-Svalbard-HS-Interannual-D-2018-2024-v2026*	Interannual	Descending	20180727 20240905	2232	60	179	60230

Table 6. List of Kapp Linné (KL) products, available in the InSAR Svalbard WebGIS (underlined names) and the Zenodo data package (*italic names*). Start and end dates of the time series are shown in YYYYMMDD format (YYYY = year, MM = month, DD = day). Abbreviations: ifgs = interferograms, doc. = documented, acqu. = acquisition.

Dataset name in the WebGIS and *CSV data package*	Product type	SAR geometry	Start date End date	Duration (days)	# acqu. dates	# used ifgs	# doc. pixels
KL Seasonal Ascending 2016 *InSAR-Svalbard-KL-Seasonal-A-2016-v2026*	Seasonal	Ascending	20160703 20161031	120	14	37	168490
KL Seasonal Ascending 2017 *InSAR-Svalbard-KL-Seasonal-A-2017-v2026*	Seasonal	Ascending	20170628 20171119	144	24	79	171675
KL Seasonal Ascending 2018 *InSAR-Svalbard-KL-Seasonal-A-2018-v2026*	Seasonal	Ascending	20180623 20181009	108	19	79	174453
KL Seasonal Ascending 2019 *InSAR-Svalbard-KL-Seasonal-A-2019-v2026*	Seasonal	Ascending	20190706 20191016	102	18	75	172164
KL Seasonal Ascending 2020 *InSAR-Svalbard-KL-Seasonal-A-2020-v2026*	Seasonal	Ascending	20200618 20201028	132	23	88	189928
KL Seasonal Ascending 2021 *InSAR-Svalbard-KL-Seasonal-A-2021-v2026*	Seasonal	Ascending	20210719 20211011	84	15	58	190174
KL Seasonal Ascending 2022 *InSAR-Svalbard-KL-Seasonal-A-2022-v2026*	Seasonal	Ascending	20220626 20220906	72	7	13	186215
KL Seasonal Ascending 2023 *InSAR-Svalbard-KL-Seasonal-A-2023-v2026*	Seasonal	Ascending	20230621 20231007	108	8	10	96599
KL Seasonal Descending 2018 *InSAR-Svalbard-KL-Seasonal-D-2018-v2026*	Seasonal	Descending	20180621 20181007	108	19	83	191262
KL Seasonal Descending 2019 *InSAR-Svalbard-KL-Seasonal-D-2019-v2026*	Seasonal	Descending	20190628 20191020	114	18	78	209126
KL Seasonal Descending 2020 *InSAR-Svalbard-KL-Seasonal-D-2020-v2026*	Seasonal	Descending	20200610 20201107	150	26	87	193410
KL Seasonal Descending 2021 *InSAR-Svalbard-KL-Seasonal-D-2021-v2026*	Seasonal	Descending	20210711 20211015	86	17	72	207388
KL Seasonal Descending 2022 *InSAR-Svalbard-KL-Seasonal-D-2022-v2026*	Seasonal	Descending	20220624 20221010	108	9	19	189119
KL Seasonal Descending 2023 *InSAR-Svalbard-KL-Seasonal-D-2023-v2026*	Seasonal	Descending	20230619 20230923	96	9	18	118263
KL Seasonal Descending 2024 *InSAR-Svalbard-KL-Seasonal-D-2024-v2026*	Seasonal	Descending	20240613 20241011	120	11	21	164333
KL Interannual Ascending 2018–2024 *InSAR-Svalbard-KL-Interannual-A-2018-2024-v2026*	Interannual	Ascending	20180804 20240919	2238	54	175	204376
KL Interannual Descending 2018–2024 *InSAR-Svalbard-KL-Interannual-D-2018-2024-v2026*	Interannual	Descending	20180802 20240905	2228	56	187	227005

3.3. Data format

The InSAR Svalbard pilot products are available in a WebGIS tool (svalbard.insar.no) and as CSV files in the Zenodo repository (Bredal et al., 2026; doi.org/10.5281/zenodo.18442696). Similar to the WebGIS structure (see **Section 4**), the Zenodo files are organised into subfolders based on the product types (seasonal and interannual) and the SAR geometries (ascending and descending). In total, 87 files are provided: 77 seasonal products (37 ascending and 40 descending) and 10 interannual products (5 ascending and 5 descending).

Each CSV file has the same naming convention:

InSAR-Svalbard-<Short name>-<Product type>-<SAR geometry>-<year(s)>-<version>.csv

- **<Short name>**: LY for Longyearbyen, NY for Ny-Ålesund, SV for Svea, HS for Hornsund, KL for Kapp Linné.
- **<Product type>**: Seasonal, Interannual.
- **<SAR geometry>**: A for ascending, D for descending.
- **<year(s)>**: YYYY for the year of seasonal products, YYYY-YYYY for the start-end years of interannual products.
- **<version>**: v2026.

The coordinates of each measurement correspond to the centre of the ~30 m pixel. Each measurement location includes positioning, topographic and data quality information, key angles describing the LOS measurement geometry and InSAR displacement metrics. All products contain the following attributes grouped here according to their primary function:

1) WebGIS reference name and identifier

- **Dataset** – Name of the dataset as displayed in the InSAR Svalbard (WebGIS only).
- **Point ID** – Unique identifier assigned to each documented pixel (WebGIS only)

2) Spatial positioning

- **east / north** – Projected pixel centre position in UTM Zone 33 (EPSG:32633). Unit: meter.
- **longitude / latitude** – Geographic pixel centre position in WGS84 (EPSG:4326). Unit: degree.

3) Topographic information

- **elevation** – Mean elevation of the pixel based on the 20 m Norwegian Polar Institute DEM (NPI, 2014). Unit: meter.
- **slope** – Mean slope angle of the pixel, based on the 20 m Norwegian Polar Institute DEM (NPI, 2014). Unit: degree.

4) Data quality information

- **coherence** – Mean coherence, ranging from 0 to 1, as indicator of the InSAR signal quality. Low coherence values suggest that decorrelation sources reduce the reliability of the displacement estimate. Unitless.
- **demerr** – SBAS-based elevation error, defined as the difference between the elevation estimated from the InSAR measurements and the external DEM (NPI, 2014). Unit: meter.

5) Measurement geometry

- **los_up** – Vertical component of the LOS unit vector. The values are negative because the satellite is looking down towards the ground. The closer to -1, the higher the sensitivity to vertical movement. Unitless.
- **los_east** – Eastern component of the LOS unit vector. The values are between -1 (west-looking) and +1 (east-looking). The closer to -1 or +1, the higher the sensitivity to east–west movement. Unitless.
- **los_north** – Northern component of the LOS unit vector. The values are between -1 (south-looking) and +1 (north-looking). The closer to -1 or +1, the higher the sensitivity to north–south movement. Unitless.
- **track_angle** – Direction of the satellite flight (counterclockwise, relative to north). Values between -25 and -18 indicate an ascending orbit. Values between -163 and -156 indicate a descending orbit. The radar azimuth direction looks 90 degrees to the right from the flight direction. Unit: degree.
- **incidence_angle** – Angle between the radar LOS and the normal (perpendicular) to the Earth's surface. Unit: degree.

The InSAR displacement information includes different variables for the seasonal and the interannual products:

1) InSAR displacement metrics for the seasonal products

- **maxdisp** – Maximum value of the InSAR displacement time series, along the radar LOS. The value expresses the relative maximum within the documented period. Unit: mm.
- **doymax** – Day of Year (DOY) of the identified maximal seasonal displacement value. Unitless.
- **YYYYMMDD** – Cumulative InSAR displacement time series with acquisition dates in YYYYMMDD format (YYYY = year, MM = month, DD = day), corresponding to the sensor-to-ground distance changes, relative to the first acquisition date of each season. The time series documents the short-term changes in surface displacement throughout the season. Unit: mm.

2) InSAR displacement metrics for the interannual products

- **trend** – Interannual mean velocity, representing the long-term linear trend of the interannual InSAR displacement time series, along the radar LOS. Unit: mm/yr.
- **YYYYMMDD** – Cumulative InSAR displacement time series with acquisition dates in YYYYMMDD format (YYYY = year, MM = month, DD = day), corresponding to the sensor-to-ground distance changes, relative to the first acquisition date in summer 2018. The time series documents the long-term changes in surface displacement between 2018 and 2024. Unit: mm.

4. InSAR Svalbard WebGIS tool

4.1. General WebGIS layout

The InSAR Svalbard GMS is openly available at svalbard.insar.no. The service consists of a web-based 3D visualisation (WebGIS) to explore the products. The WebGIS interface includes six main elements for data navigation, visualisation, and basic analysis (**Figures 4–5**):

- **Map viewer:** The map can be shown in both 2D and 3D modes (**Figure 5**, tool H). The 3D mode is especially helpful when examining mountainous terrain.
- **North arrow and scale:** In 2D mode, the north arrow is fixed and consistently pointing upwards. In 3D mode, it dynamically rotates according to the current viewing direction. The scale bar, displaying distances in meters or kilometres, updates automatically depending on the zoom level**.**
- **Coordinates:** Coordinates and elevation are displayed at the bottom of the interface when clicking anywhere on the map viewer. By default, coordinates are shown in latitude/longitude (WGS84), but users can switch to UTM 33 (meters) by clicking the coordinate display. A window containing more details about data and code attributes opens when clicking the blue 'About data…' link.
- **Map layers:** The list of available background layers and InSAR products is available in the upper left corner. Users can (un)select the datasets they want to view on the map.
- **Toolbar:** The bar in the upper-right corner provides additional information and tools for navigation, data visualisation, dataset selection, and basic analysis (**Figure 5** and **Table 7**).
- **Legend**: The legend window is open by default and shows the colour scale and visualisation parameters applied to the displayed InSAR products. These settings can be modified by the user. The legend window can be closed by using the "X" in the upper-left corner and reopened by clicking the legend icon in the toolbar (**Figure 5**, tool D).

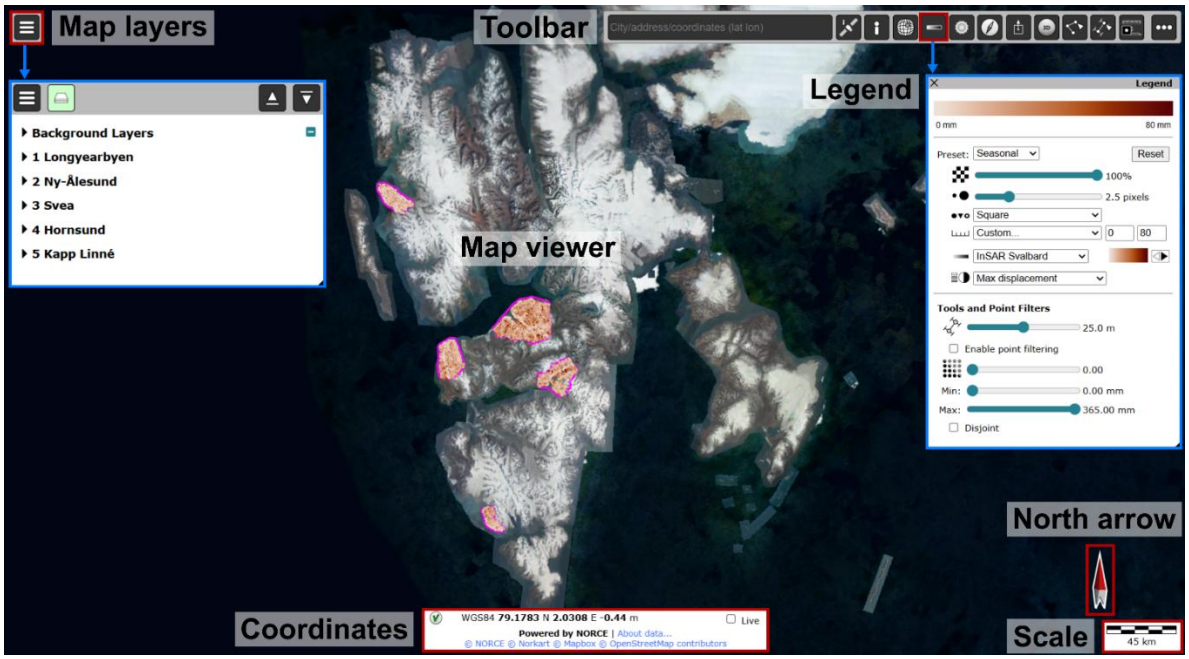

Figure 4. General layout of the WebGIS interface. The red rectangles show the six main elements of the visualisation tool. The blue boxes display the opened map layers panel and legend window. Background: Svalbard Orthophoto (NPI, 2026b) and NASA Blue Marble.

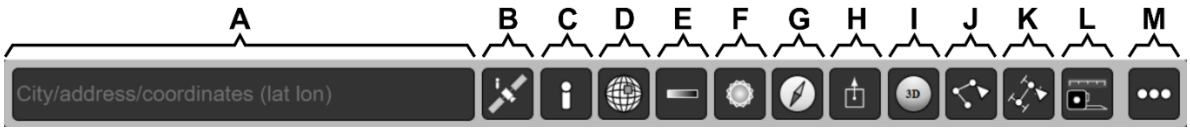

Figure 5. Toolbar available in the upper-right corner of the WebGIS interface (**Figure 4**). The labels A–M are explained in Table 7.

Table 7. Description of toolbar elements available in the WebGIS interface. The icons corresponding to the tool labels are shown in **Figure 5**.

Tool Label	Tool Function
A	Search by location name, address, or geographic coordinates (latitude/longitude).
B	Open an information window explaining main InSAR Svalbard properties and limitations
C	Open an information window explaining the WebGIS structure and navigation
D	Add external layers via Web Map Service (WMS) servers.
E	Show or hide the dataset legend.
F	Adjust light direction according to the current view angle (3D mode only).
G	Display the user's current location on the map (requires browser permission).
H	Generate a shareable link to the current map view.
I	Toggle between 2D and 3D display modes.
J	Draw a polygon to spatially average InSAR time series.
K	Create a cross-section to visualise displacement time series along a profile.
L	Measure horizontal distances.
M	Show or hide the toolbar.

4.2. WebGIS navigation

The WebGIS interface allows the user to pan, zoom, tilt, and rotate the map. In 2D mode, it is possible to fly in/out, left/right and up/down. To tilt and rotate, the user must first activate the 3D mode in the toolbar (**Figure 5**, tool I). The navigation can be performed using a mouse, a keyboard or a touch screen. The possible actions are summarised in **Table 8**. Other navigation tips are provided by clicking the information icon in the toolbar (**Figure 5**, tool C).

The toolbar includes a geographical search function (**Figure 5**, tool A) that allows for quickly move to an area of interest by entering a location name or latitude/longitude coordinates.

Table 8. Actions for InSAR Svalbard WebGIS navigation.

Action	Mouse	Key	Touch
Fly in / out (2/3D modes)	Scroll wheel on mouse or scroll gesture on trackpad	W, S	Stretch/Pinch with two fingers
Fly left / right (2/3D modes)	Click-and-drag	A, D	Drag with one finger
Fly up / down (2/3D modes)	Click-and-drag	Q, E	Drag with one finger
Tilt (3D mode only)	Click-and-drag with right mouse button or while holding Shift key	-	Move two fingers up or down
Rotate (3D mode only)	Click-and-drag with right mouse button or while holding Shift key	-	Move two fingers in a circular motion
Enter / Exit free-flight mode	-	Alt + G	-

4.3. Background layers

The default view displays NASA's Blue Marble optical imagery as base layer, and Norwegian Polar Institute orthomosaics above it (NPI, 2026b). A pink vector layer indicates the locations of the InSAR Svalbard study areas.

The map layers panel includes additional background layers that the users can choose to (un)select (**Figure 6**). Each dataset can be (de)activated by clicking the icon next to its name. Layers marked with a black cross are currently inactive and therefore not displayed in the map viewer.

For comparing InSAR data with other datasets, external vector layers (points, lines and polygons) can be imported by dragging GEOJSON files into the map viewer (**Figure 7**). The initial files must be in the EPSG:4326 coordinate reference system (WGS 84). Additional Web Map Service (WMS) layers can be added through the toolbar (**Figure 5**, tool D).

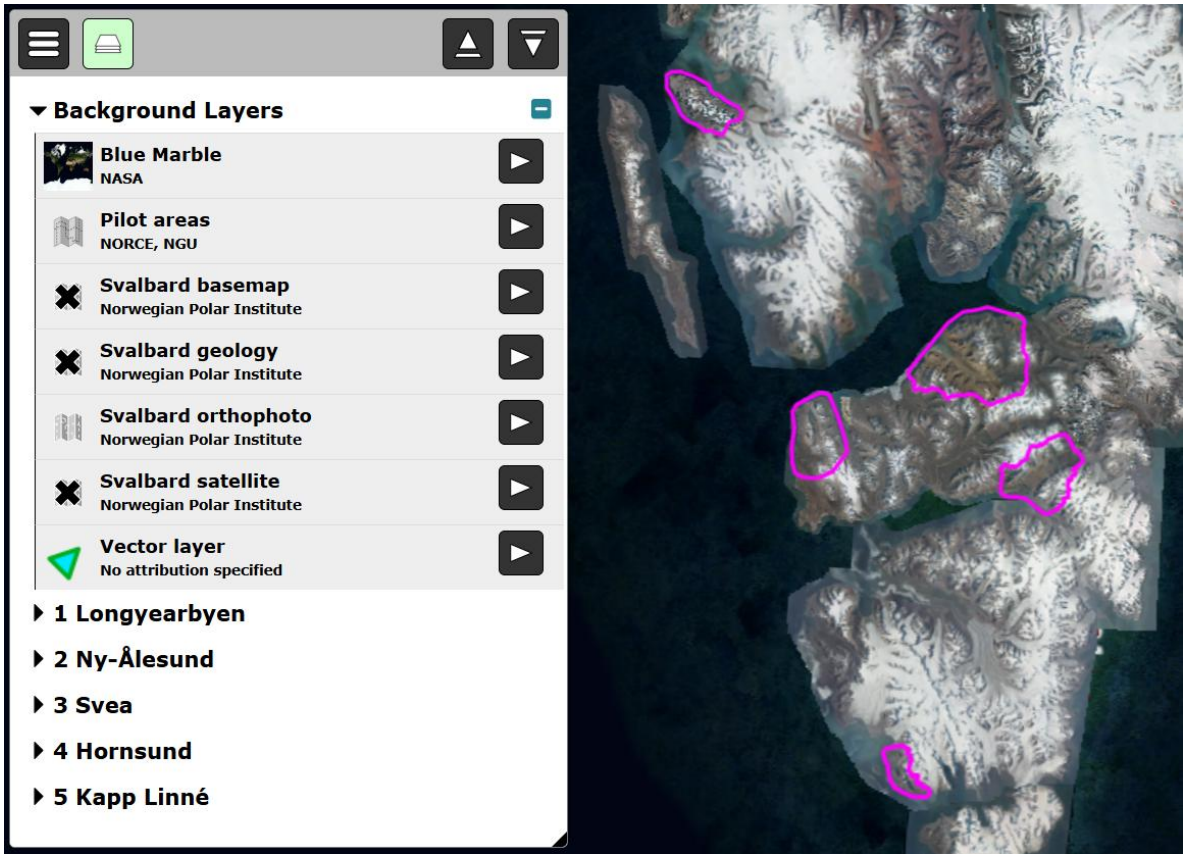

Figure 6. Background layers and default visualisation in the WebGIS interface. Background: Svalbard Orthophoto (NPI, 2026b) and NASA Blue Marble.

Figure 7. Importing external vector layers into the WebGIS. When dragging GEOSJON WGS84 files into the WebGIS interface, the vectors get listed in the map layers panel and displayed as pink points, lines or polygons in the map viewer. Background: Svalbard Orthophoto (NPI, 2026b).

4.4. Map viewer

The menu in the upper-left panel of the WebGIS interface (**Figure 4**) provides access to the InSAR Svalbard products (see **Section 3.2**). The products are grouped into five main categories corresponding to the study areas. Within each group, datasets are organised by product type (seasonal or interannual) and SAR viewing geometry (ascending or descending). When a dataset is selected, the InSAR measurements are displayed as coloured squares in the map viewer (**Figure 8**).

Each dataset is enabled by selecting the checkbox on the left in the product list (**Figure 9**, blue circles). Multiple datasets can be viewed simultaneously. All layers within a group can be activated at once by selecting the checkbox next to the group header (**Figure 9**, green circles) or by clicking the group while holding the Alt key. The full spatial extent of a dataset can be visualised by clicking the arrow next to the dataset name (**Figure 9**, purple circle)

Depending on the product type, the colours of the squares displayed on the map either represent the seasonal maximum LOS displacement (attribute 'maxdisp', in mm), or the interannual LOS velocity (attribute 'trend', in mm/year). Different default colour scales and ranges are used to distinguish between these two product types and their respective units (**Figure 10**). The seasonal products are visualised with a sequential colour scale ranging from 0 to 80 mm. The interannual products are visualised with a diverging colour scale range from -20 to +20 mm/yr. Legend settings can be adjusted separately for seasonal and interannual data by selecting the correct product type in the Preset menu (**Figure 10**, orange circle). Changes made in the legend panel will only affect the currently selected data type, allowing different legend settings for each product.

The legend panel includes many functions allowing the user to customize the size and shape of the measurement locations and change the palette and range of the colour scale to the different presets. It is also possible to select other attributes to be mapped, and to apply thresholds to filter out the displayed data based on the coherence (InSAR quality measure) or the minimum/maximum displacement/velocity (**Figures 10–11**). At any time, the user can go back to the default settings using a 'Reset' function.

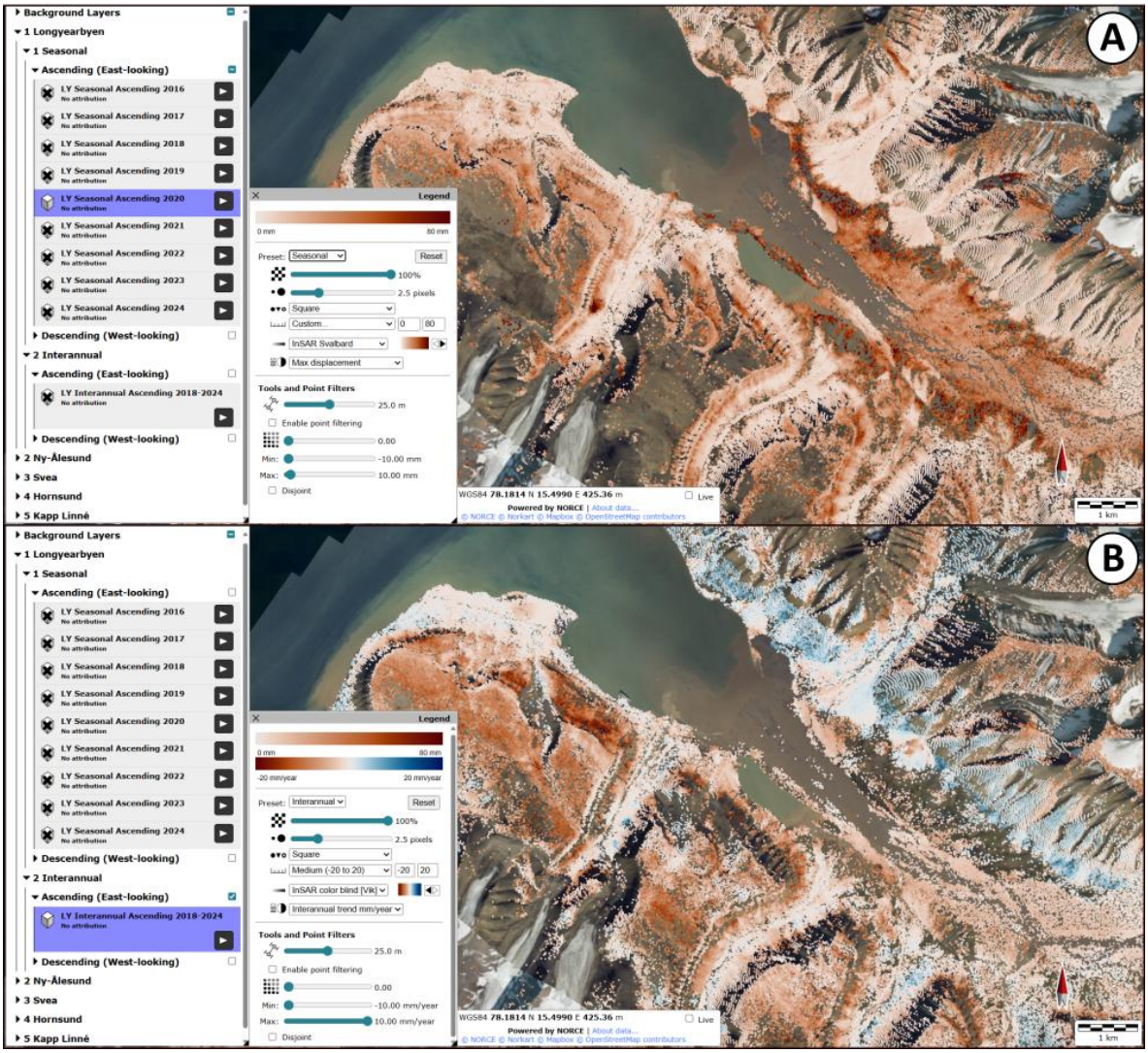

Figure 8. Product visualisation in the WebGIS in the Longyearbyen study area. Products highlighted in purple-blue have been activated using the checkbox left from the layer name. **A.** Seasonal product. The map shows the maximal displacement during the selected season (mm). **B.** Interannual product. The map shows the interannual velocity trend between 2018 and 2024 (mm/yr). The colour scale and visualisation settings can be modified in the legend panel. Background: Svalbard Orthophoto (NPI, 2026b).

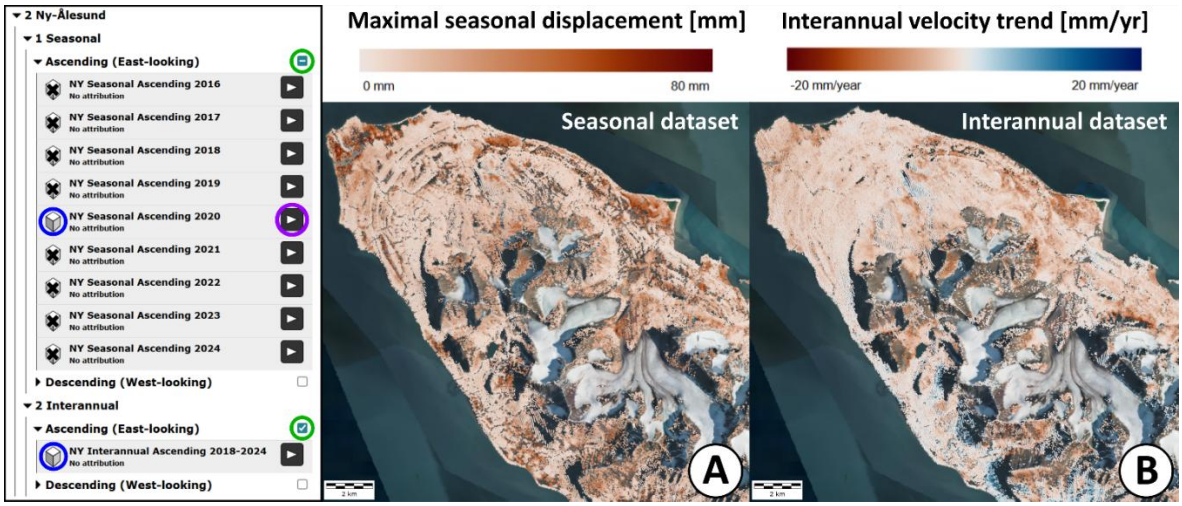

Figure 9. Dataset selection and visualisation in the WebGIS interface. Individual layers can be activated by clicking the dataset icon (blue circles). All layers within a group can be toggled via the group checkbox (green circle) or by clicking the group while holding the Alt key. The arrow next to each dataset (purple circle) allows users to display the full spatial extent of the selected layer. **A.** Default visualisation of the seasonal product (sequential scale ranging from 0 to 80 mm). **B.** Default visualisation of the interannual products (diverging scale ranging from -20 to +20 mm/yr). Background: Svalbard Orthophoto (NPI, 2026b).

Figure 10. Visualisation functions in the legend panel (1). The visualisation settings vary for the two product types (seasonal and interannual) according to the selected Preset (orange rectangle) **A.** Example based on a seasonal product, where the user has increased the square size to 6.0 (green rectangle), increased the contrast of the map using a custom range between 0 and 50 mm (purple rectangle) and filtered out low coherence measurements (light blue rectangle). **B.** Example based on an interannual product, where the user has increased the square size to 6.0 (green rectangle), increased the contrast of the map using a fine scale (purple rectangle) and filtered out positives values to only focus on measurements corresponding here to a subsidence (pink rectangle). To go back to the default settings, the user can use a 'Reset' function (dark blue rectangle). Background: Svalbard Orthophoto (NPI, 2026b).

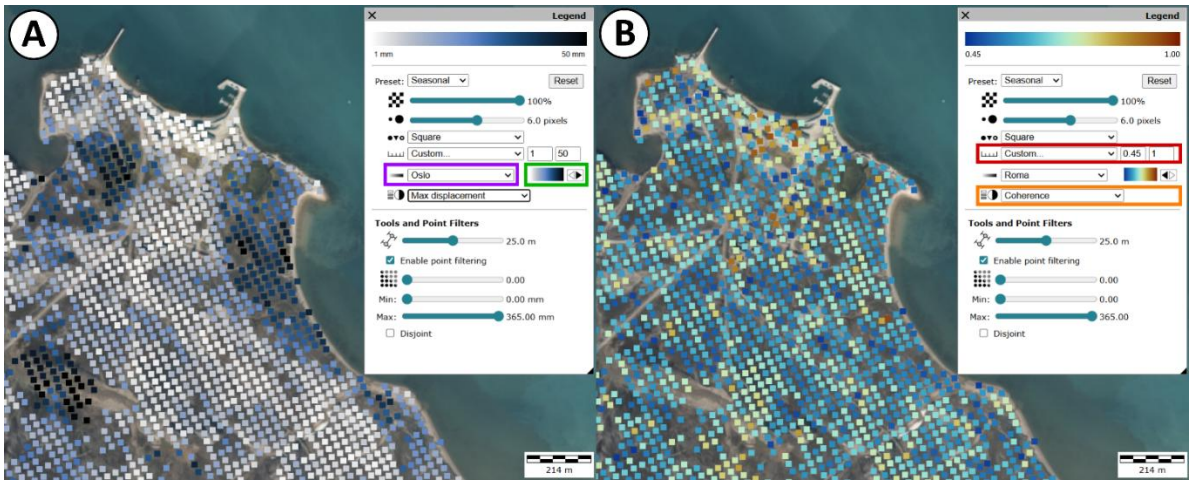

Figure 11. Visualisation functions in the legend panel (2). **A.** Alternative colour palettes can be chosen by the user (purple rectangle). The arrows on the right from the colour scale can be used to flip the palette (green rectangle). **B.** Other variables can be mapped, such as the coherence (InSAR quality measure) (orange rectangle). The scale range has been manually adjusted according to the minimum–maximum values of the chosen variable (0.45–1 for coherence of the seasonal products) (red rectangle). Yellow to red pixels on the map show areas with high signal stability, relatively to the surroundings (blue pixels). Background: Svalbard Orthophoto (NPI, 2026b).

4.5. Time series viewer

Displacement time series and associated information about the measurement properties can be accessed either by selecting an individual InSAR pixel or by drawing a polygon to average multiple pixels (**Figure 5**, tool J). Once selected, the corresponding location is automatically highlighted on the map (**Figure 12**, dark blue rectangle), and the time series viewer (**Figure 12**, pink rectangle) opens simultaneously, displaying the LOS InSAR displacement evolution over time.

The time series viewer provides functions to retrieve information about the measurement properties, to view all variables associated to the selected pixel(s), and to plot the displacement against time:

- **Basic metadata**: The dataset name, Point ID, position, coherence and main displacement metrics (max displacement and its DOY or interannual trend), are listed in the upper-left (**Figure 13**, red rectangle). The SAR acquisition geometry and the corresponding LOS measurement direction are documented in the upper-right (**Figure 13**, orange rectangle).
- **Axis rescaling:** The graph shows the measured displacement (y-axis) against the acquisition time (x-axis). By default, the axes are scaled to see the entire documented period and all displacement values. The viewer is interactive, and the user can zoom and rescale axes by using the mouse or touchpad gestures. To rescale only the y-axis, zoom in/out while holding the Shift-key. Fixed y-axis limits can also be set by selecting specific values in a scrolling menu at the bottom of the viewer (**Figure 13**, light blue rectangle). To rescale the x-axis only, zoom in/out while holding the Ctrl-key. The default view can be restored by using the 'Fit' function**.**
- **Display options**. Time series can be visualised either as discrete points corresponding to each acquisition date or by connecting the acquisitions with lines (**Figure 13**, green rectangle). A denser x-axis grid can be displayed and adjusted by activating the 'Dense grid' checkbox. The

'Ambiguity' checkbox shows how the time series would shift by +/- half the wavelength (28 mm), which can help identify potential biased values.

- **Trend analysis**: Several best-fit functions (e.g., linear for slope movements, polynomial for non-linear seasonal thaw–freeze cycles of the active layer) can be applied to display the main displacement trend (**Figure 13**, pink rectangle).
- **Tabular view**: The data option (**Figure 13**, dark blue rectangle) allows for tabular access to all attributes associated to the selected pixel (see **Section 3.3**). When pixels are averaged within a polygon, the table shows the averaged values.

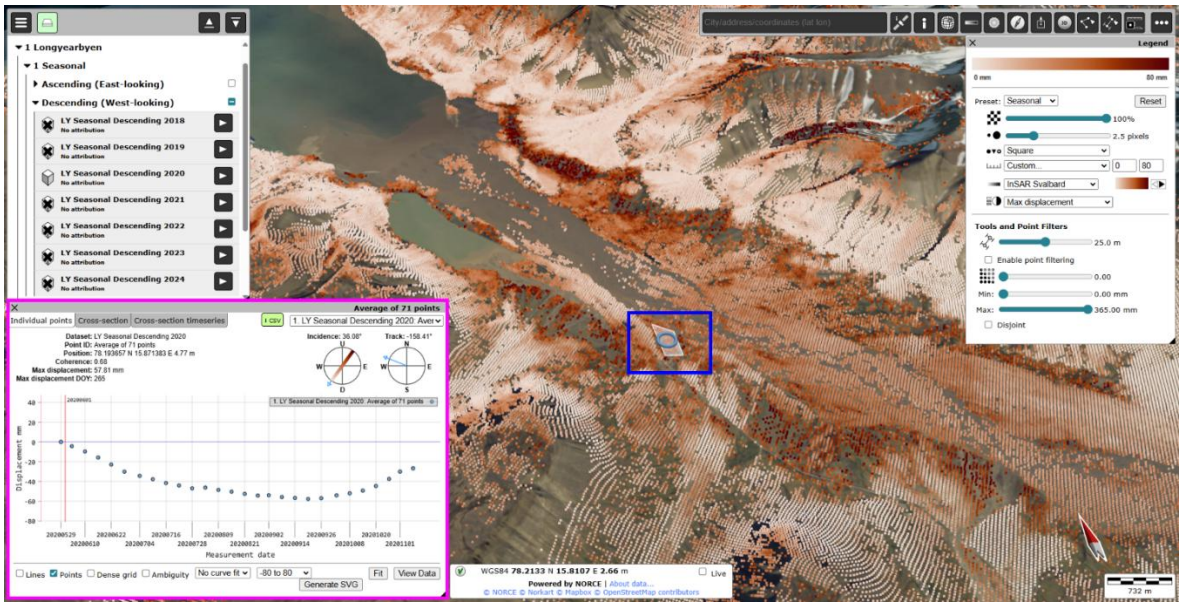

Figure 12. InSAR seasonal time series in the WebGIS interface. A polygon can be drawn for pixel averaging (dark blue rectangle) and the resulting averaged displacement time series gets plotted in the Time series viewer (pink rectangle). Background: Svalbard Orthophoto (NPI, 2026b).

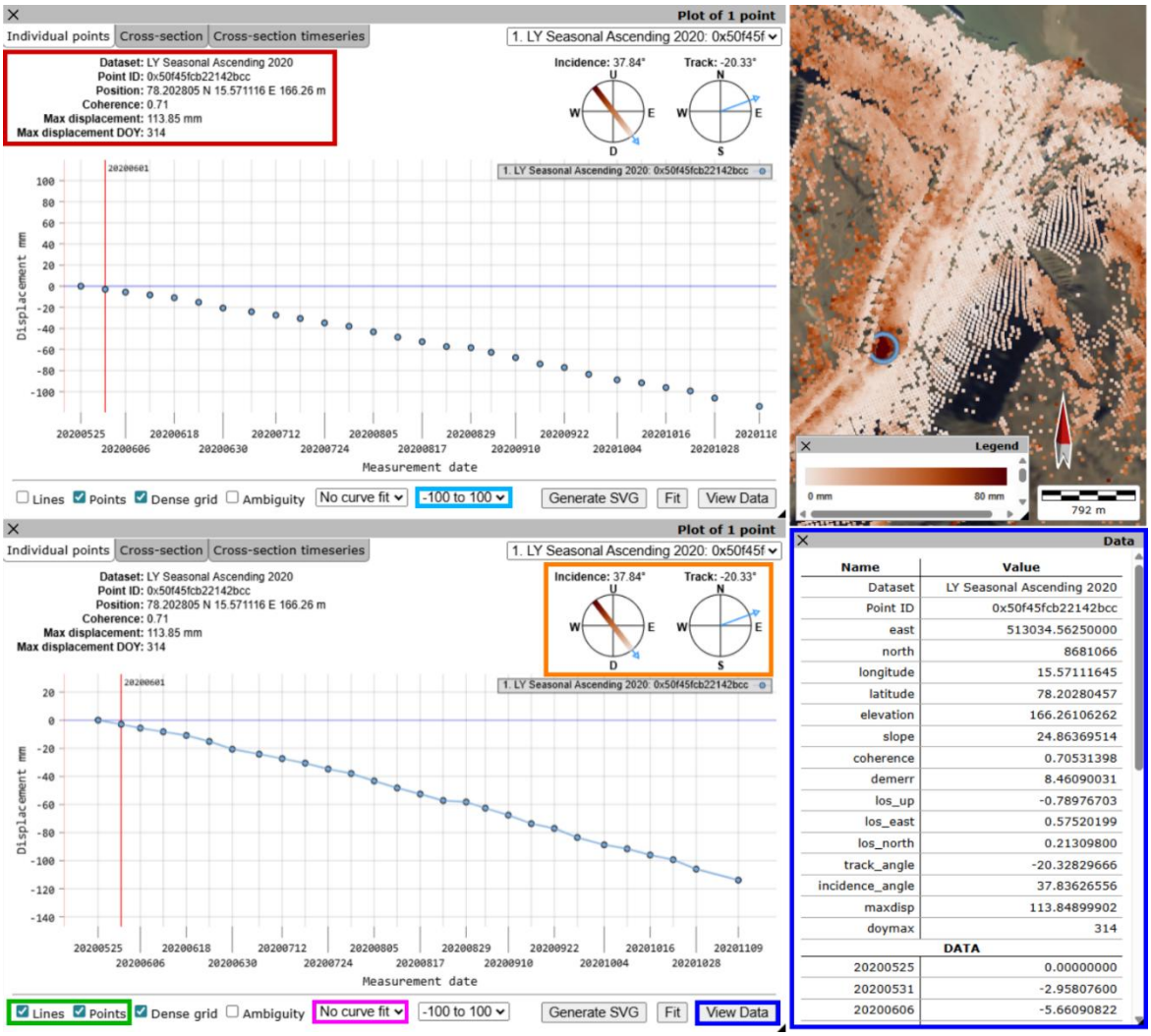

Figure 13. Time series viewer displaying displacement plotted against time. The viewer includes other key information and functions: general information of the point (red rectangle); information about satellite viewing direction (orange rectangle); optional fixed y-axis scale (light blue rectangle); view data and connect acquisitions with lines (green rectangle); optional best-fit function (pink rectangle); tabular view showing all attributes associated to the selected pixel (dark blue rectangle). Background: Svalbard Orthophoto (NPI, 2026b).

Time series from multiple datasets (several years and/or viewing geometries) can be plotted together for comparison. All desired products must first be selected in the map layer panel and are then overlaid in the map viewer. Time series from multiple pixels can also be compared by selecting additional locations while holding the Shift-key. In this mode, the time series window updates to display the information of the most recently selected pixel, while retaining the first series plotted in the viewer (**Figure 14**). The information related to the first selected pixel remain accessible in the scrolling list in the upper right (**Figure 14**, dark blue rectangle).

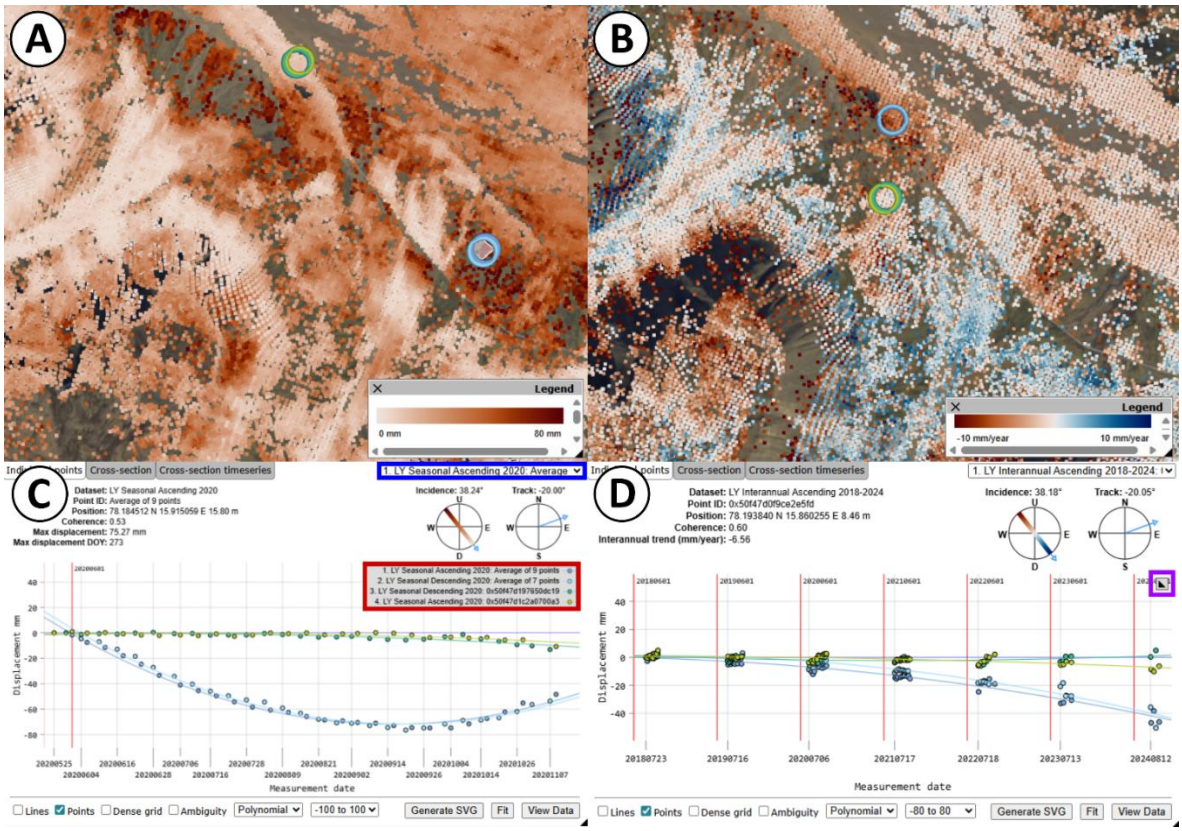

Figure 14. Comparison of time series from different geometries and different locations. **A–B**: locations of two polygons or single pixels selected while holding the Shift key. **A.** Seasonal products. **B.** Interannual products. All circled locations are selected for plotting time series. Background: Svalbard Orthophoto (NPI, 2026b). **C.** Seasonal time series in 2020, comparison to the locations shown in A. **D.** Interannual patterns between 2018 and 2024, corresponding to the locations shown in B. Information listed at the top of the time series viewer correspond to the last selected location, while the previous ones can be accessed by scrolling the list in the upper-right (dark blue rectangle). The datasets used are listed in the graph legend (red rectangle), that can be hidden by the user when clicking on it (purple rectangle).

The cross-section tool (**Figure 15**, A, yellow rectangle) enables visualisation of the InSAR results along user-defined transects. The cross-section viewer (**Figure 15**, B) plots the maximal displacement (for seasonal) or the velocity (for interannual) along the transect. The cross-section time series viewer (**Figure 15**, C) displays the temporal evolution of displacement along the transect over the observation period using a graduated colour scale, where each line represents an acquisition date. The user can modify the transect width (**Figure 15**, A, dark blue rectangle) and customised the colour scale and plot visualisation (**Figure 15**, green rectangle).

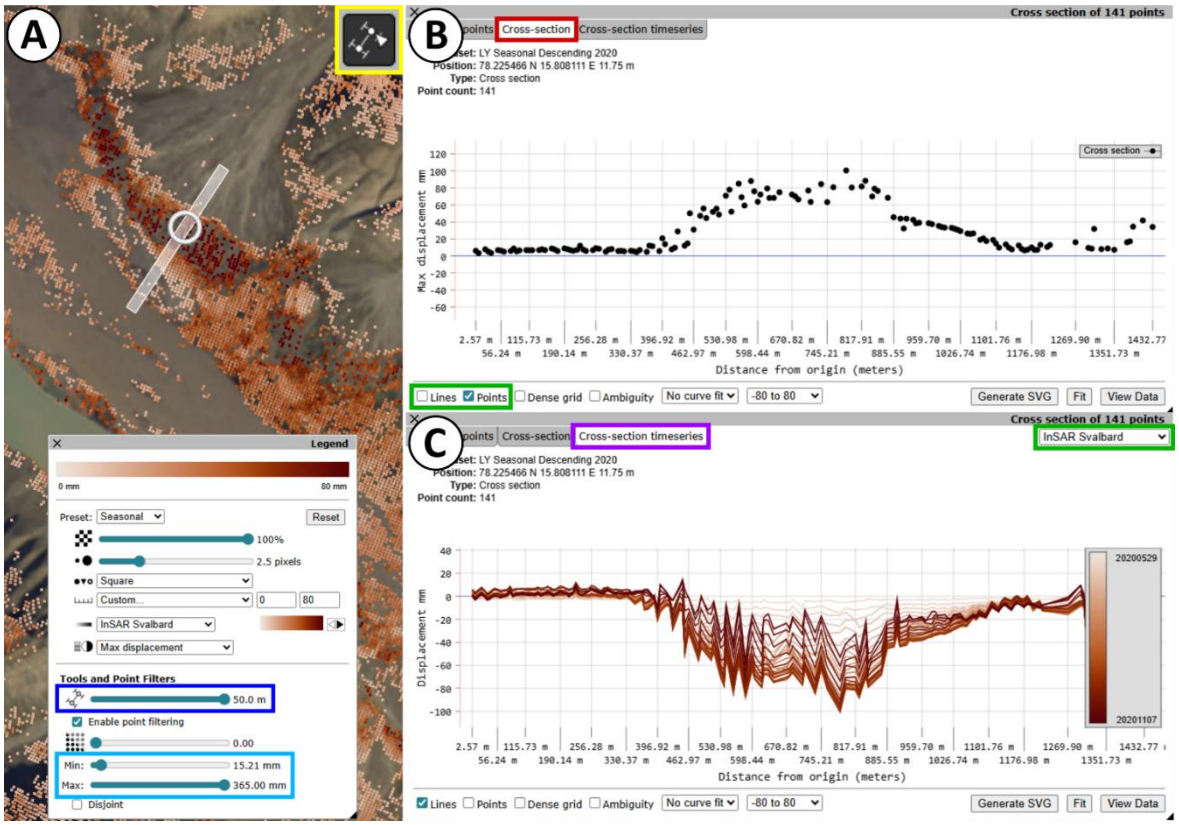

Figure 15. Cross-section function. **A.** The user first draws a transect on the map (here along an alluvial fan) with the cross-section tool (yellow rectangle). The width of transect to average the InSAR measurements can be adjusted (default: 25 m) (dark blue rectangle). The pixels visualised on the map can be filtered according to displacement thresholds (light blue rectangle). Background: Svalbard Orthophoto (NPI, 2026b). **B.** The displacement values from the map are displayed along the section using the cross-section panel (red rectangle). **C.** The time series can also be visualised using the cross-section timeseries panel (purple rectangle). The visualisation of the graphs can be customized (green rectangles).

4.6. Data sharing and download

A sharable URL link with the current map view can be created by clicking on the square icon in the toolbar (**Figure 5**, tool H). The link can be saved and shared to view the same location and layer selection in the map viewer (**Figure 16**, B).

The data from several pixels can be downloaded by drawing a polygon and clicking the CSV button at the top of the time series viewer (**Figure 16**, A, dark blue rectangle). The time series plot can be downloaded as SVG file (**Figure 16**, A, purple rectangle). The values displayed in the data viewer table (single measurement or averaged value) can be downloaded by scrolling down to the end of the table and clicking the CSV button (**Figure 16**, C, green rectangle).

For downloading full-resolution InSAR Svalbard data, an Application Programming Interface (API) similar to InSAR Norway GMS is also available (insar.ngu.no/api-docs/api/).

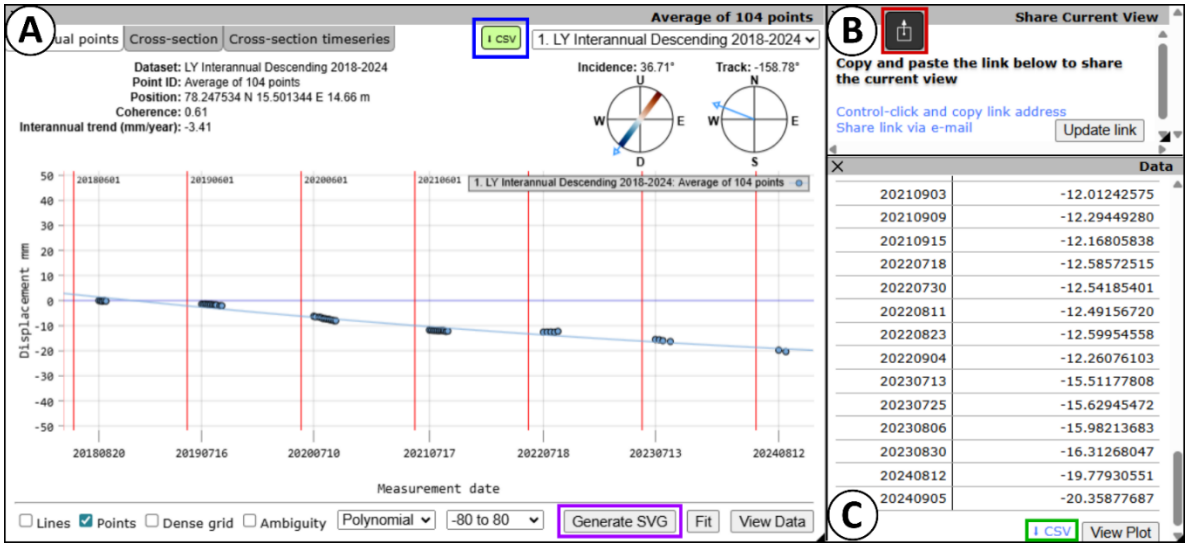

Figure 16. InSAR Svalbard data sharing and download. **A.** The CSV button at the top of the time series viewer downloads the data from one selected pixel or several pixels within a drawn polygon (dark blue rectangle). The SVG button saves an image of the time series plot (purple rectangle). **B.** The sharing tool (red rectangle) creates a sharable URL link of the current map view. **C.** Data from a single point or the average of several points can be downloaded with the CSV button at the end of the data viewer (green rectangle).

5. InSAR Svalbard data interpretation

5.1. Limitations and uncertainties

The InSAR Svalbard products are subject to several uncertainties and limitations inherent to InSAR processing (see **Section 2**). The main challenges affecting the product quality are summarised below:

- **SAR geometry and LOS measurements:** InSAR does not capture the full three-dimensional displacement information. The radar only detects a distance change between the sensor and the ground. The documented displacement is one-dimensional along the LOS. The absence of detected movement does not imply stability. Measured values might be underestimated if the true movement direction deviates from the LOS direction.
- **Reference time and location:** InSAR is a relative technique. Temporally, all individually processed datasets are relative to the first acquisition in the series. Spatially, all results are relative to a reference location expected to be stable. Considering the difficulty for validating the stability assumption in the highly dynamic Svalbard environment lacking comparable in-situ measurements, we applied an empirical approach for selecting such references. We tested several reference locations and analysed the impact on the results (displacement shifts, differences in ascending and descending). The final locations correspond to buildings (in Longyearbyen and Ny-Ålesund), to a coarse and inactive part of an alluvial fan (in Svea) or to bedrock outcrops (in Hornsund and Kapp Linné) (**Table 1**). The users must be aware that if movement is affecting the chosen locations, the results might be shifted. Especially for Svea, the reference point selection was challenging, due to movement affecting most of the documented surfaces. The chosen location is not ideal, but it was the most stable option we could identify at this stage. If the reference is affected by long-term subsidence or creep, this might have caused displacement shifts for the other pixels.
- **Atmospheric and ionospheric effects:** Atmospheric effects are considered the main error sources for most InSAR applications. At high latitudes, phase delays due to ionospheric effects also have a significant impact on data quality, even for C-band radars. Ionospheric effects sometimes lead to major phase shifts at the limits between bursts. Interferograms affected by such issues have been discarded. The SBAS approach uses the temporal redundancy of overlapping interferograms to mitigate tropospheric effects. Despite the processing strategies to mitigate these effects, atmospheric and ionospheric delays can still affect the results, especially when the processing includes a limited number of interferograms. The seasons with 12-day temporal resolution (2016, 2022–2024) are more vulnerable to these issues due to few exploitable images and interferograms (**Tables 2–6**). For this reason, we discarded 2024 ascending products for three study areas (**Table 1**). Errors associated with an uncorrected atmospheric component tend to increase with the distance from the reference location used for phase calibration (Emardson et al., 2003) (**Table 1**).
- **Snow, moisture and vegetation:** Wet snow causes surface decorrelation, thereby reducing the spatial coverage of the InSAR products and shortening the duration of the observation time window. Similarly, ground displacement on very moist surfaces is often not detectable, which may prevent complete InSAR data coverage of flooded valley bottoms, or slopes affected by wet mass-wasting processes (e.g., debris-flows, mudflows). In addition, the effects of scattering mechanisms in coherent areas must be considered. The differential propagation of the

electromagnetic wave due to changing dielectric properties may lead to biased phase estimates. This can occur due to snow (Antonova et al., 2016), ground moisture (Zwieback et al., 2015) or vegetation (Zwieback and Hajnsek, 2014).

- **Decorrelation, unwrapping errors and phase ambiguities:** Sentinel-1 InSAR is not well suited to document fast movement (> dm–m/yr). If a sudden and large change in the target position occurs between two consecutive acquisitions (e.g., a landslide), a coherence drop might be detected but InSAR may be unable to document the movement. Similar problems occur for gradual processes if they are too fast (e.g., glacier flow, rock glacier creep, large subsidence). With Sentinel-1 best temporal baseline (6 days), the decorrelation limit is ~170 cm/yr, but aliasing can occur when the velocity exceeds ~85 cm/yr. When using annual interferograms (340–390 days), this limit decreases to 2.6 to 3 cm/yr, and aliasing can occur when velocity exceeds 1.3–1.5 cm/yr. The filtering criteria explained in **Section 2.2** aim to discard pixels likely to be affected by phase ambiguities, but biases can remain, especially for the interannual products. The conversion of the cyclic phase changes to absolute phase changes and sensor-to-ground displacement is based on unwrapping algorithms that assume spatial continuity and gradual changes (Chen and Zebker, 2002). If movement rate is highly variable across a landform and differences between adjacent pixels exceed one fringe (half the wavelength during the selected time interval), the results might be affected by errors. Such issues are also likely to occur if the processed area is affected by major data gaps, for example due to fjords, rivers, lakes or glaciers. Large-scale unwrapping problems were mitigated by discarding the affected interferograms. Locally, however, small errors are expected, especially in mountains where small coherent areas are isolated by non-coherent areas.

These limitations have important implications for the subsequent data exploitation by the end-users. In the following sections, we provide guidance on how to interpret the spatial distribution of the results viewed as maps and the temporal evolution of the results viewed as time series.

5.2. Spatial interpretation of InSAR Svalbard maps

The seasonal maps show the maximum detected displacement of the seasonal InSAR time series. However, the total seasonal displacement may be underestimated, particularly when the thawing begins before the first reliable InSAR acquisition. In spring, coherence is commonly reduced by snowmelt and water-saturated ground conditions, which reduces the data quality. In such cases, early-season interferograms may have been discarded, leading to a partial loss of displacement information. The seasonal products are therefore best suited for identifying hotspots of deformation and assessing relative spatial patterns, rather than interpreting absolute displacement values. For users interested in the overall spatial distribution of the movement, we recommend examining first the 2017–2021 products, which have a higher quality due to better data availability and longer documented time periods.

The measurements are one-dimensional along the radar LOS and will therefore underestimate the real displacement if the movement direction deviates from the LOS. Considering the diversity of the processes and different expected movement directions, we have not projected the results. Depending on their applications and study areas, the users can apply a correction using the LOS angles documented in the dataset, e.g., vertical projection when focusing on flat permafrost terrain (Wendt et al., 2026), or downslope projection for slope processes (Cai et al., 2022).

The observation time window varies between years, typically covering May–July to September–December (**Tables 2–6**), depending on annual snow and moisture conditions. Observable inter-seasonal differences of maximum displacement are not necessarily due to variable climatic conditions or changes of ground processes, but also due to the variable documented periods. When early images needed to be discarded due to low coherence, significant underestimation of the seasonal subsidence is expected, while other seasons might be closer to the actual displacement amplitude if the series starts close to the thaw onset. Overall, users must be cautious when comparing displacement between seasons.

Each InSAR pixel integrates all surface processes occurring within its footprint (~30x30 m), e.g., slope movement, thaw subsidence, or a mixture of these processes. As a result, the measured displacement may reflect either a single dominant process, or a superposition of multiple mechanisms acting simultaneously.

Some areas are not covered by InSAR data. They either correspond to areas which are not visible to the satellite (shadow or layover effects, **Figure 17**, A, black circles) or to pixels that are filtered out due to low quality (**Figure 17**, A, coloured circles). Importantly, the absence of data does not imply an absence of movement, but that InSAR cannot be used in those areas. InSAR cannot be applied over water bodies and often decorrelates over wet surfaces (**Figure 17**, A, light blue circles) or snow-covered areas (**Figure 17**, A, green circles). Fast-moving surfaces often decorrelate and cannot be reliably documented (**Figure 17**, A, purple circles). Debris-free glaciers often combine fast movement and snow-covered surfaces and therefore remain mostly undocumented (**Figure 17**, A, dark blue circle).

Some pixels may be affected by noise, phase ambiguities, or local measurement artefacts. Randomly distributed values over short distances (“salt-and-pepper effect”, **Figure 17**, A, green circles) must be treated with caution. We recommend always jointly analysing and/or averaging several neighbouring pixels, instead of focusing on isolated individual pixels.

Interannual products display the mean velocity trend across the observation period (2018–2024; **Tables 2–6**), typically reflecting long-term subsidence associated with permafrost degradation, uplift related to ice aggradation or creep processes on slopes. Many of the limitations described for the seasonal products apply similarly. However, the spatial coverage is not identical with the seasonal products due to the different processing strategies (see **Section 2.2**). Higher pixel density is expected in areas with late-lying snow due to the use of July–September images only. Lower pixel density is expected on fast-moving landforms due to the long timespans used to connect the snow-free seasons. In addition, more unwrapping errors and phase aliasing are expected due long-time intervals used to connect the years. The users must remain critical when examining areas with movement patterns significantly different from their surroundings (**Figure 17**, B).

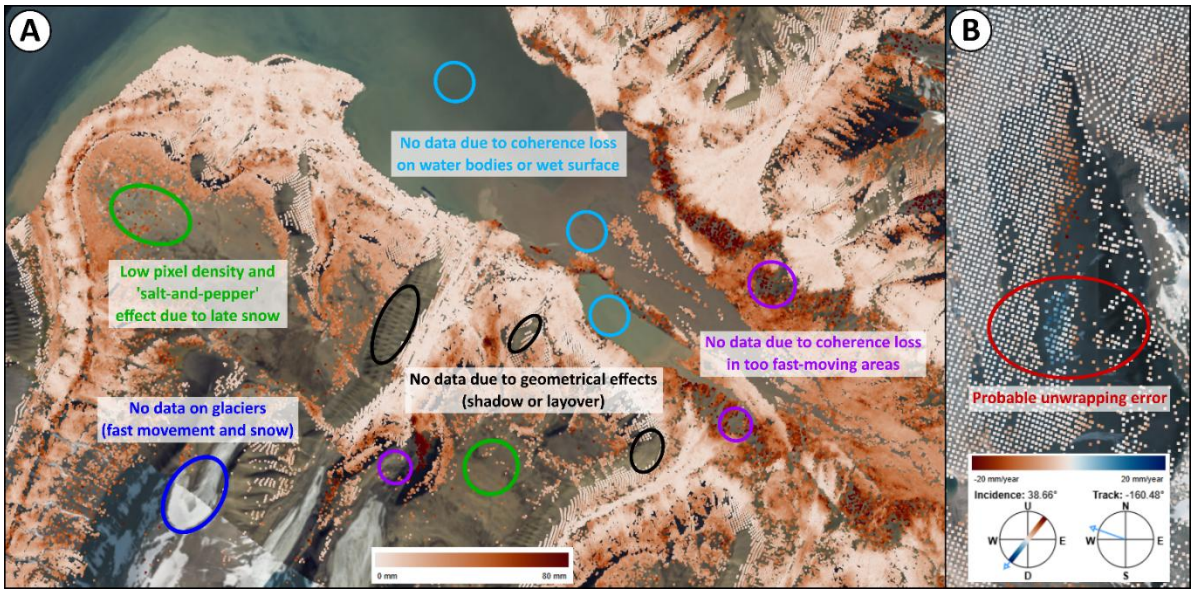

Figure 17. Common InSAR limitations. **A.** Seasonal product with areas affected by data gaps (black) or low InSAR signal quality due to fast movement (purple), wet surface (light blue), late-lying snow (green) or glaciers (dark blue). The users should avoid overrelying on single pixels, without looking at the surroundings. One should be especially careful in areas affected by 'salt-and-pepper' effects (green). **B.** Interannual product with an example of a west-facing slope likely affected by an unwrapping error. Using a descending geometry with the radar looking toward West, a movement away from the radar (negative values shown in red) is expected. A quick transition from red to blue is suspicious and probably indicates an unwrapping error over a fast-moving landform. Background: Svalbard Orthophoto (NPI, 2026b).

5.3. Temporal interpretation of InSAR Svalbard time series

The seasonal time series start at zero every year. Winter periods cannot be monitored due to snow cover, and the seasonal time series are therefore not connected as each year has been processed independently. A vertical red line is displayed in the time series window on June 1st every year to provide a similar reference (**Figure 18**). Long-term surface movement may affect some areas, but such changes cannot be identified from seasonal time series alone. Seasonal time series derived from ascending and descending geometries are not expected to align perfectly, due to differences in acquisition time and different viewing angles (**Figure 18**). Differences in displacement amplitude and spatial patterns between the two datasets are therefore expected and should be interpreted in respect to the LOS of each dataset.

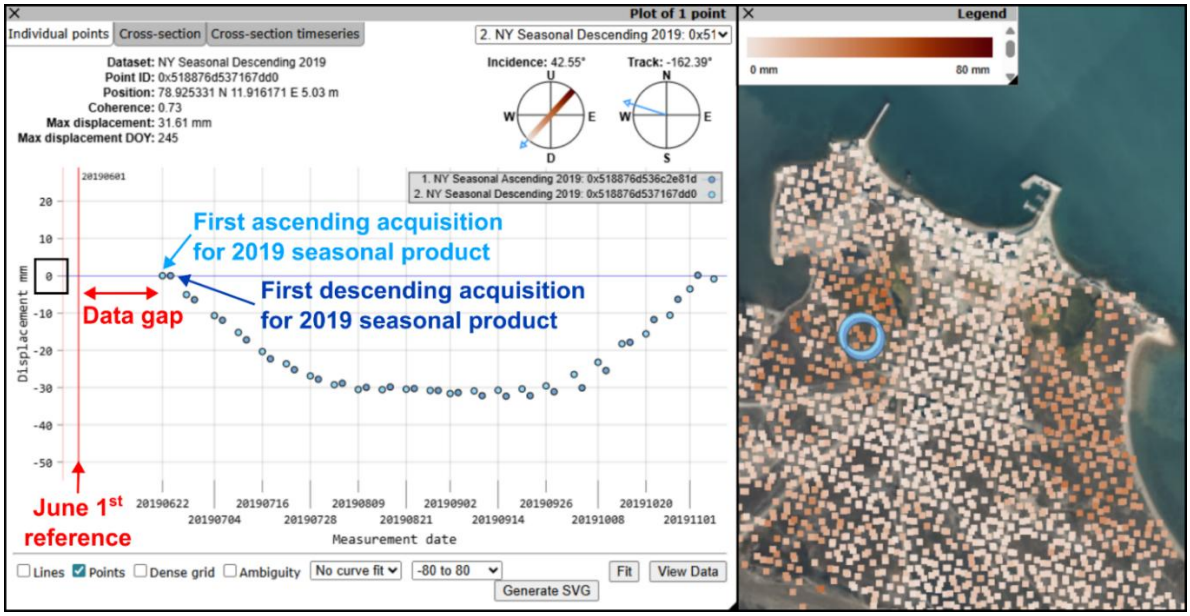

Figure 18. Temporal references in seasonal products. The acquisition times in ascending and describing orbits are slightly shifted. Both displacement time series start at zero, relative to their respective first acquisition. A vertical red line set on June 1st is displayed for all years, to support the visual comparison between products. Background: Svalbard Orthophoto (NPI, 2026b).

The users must remain critical when looking at the time series. Displacement shifts of several centimetres between consecutive acquisitions usually indicate phase ambiguities. The users should avoid overrelying on single-pixel time series without carefully analysing the surroundings. Averaging several points within a polygon (**Figure 5**, tool I) is a valuable way to provide more robust estimates of seasonal displacements and to avoid focusing on unrepresentative patterns.

Comparisons between several geometries and years is a valuable way to confirm the consistency of the measured patterns or identify outliers (**Figure 19**). In flat terrain, where the seasonal displacement is expected to highlight a cyclic pattern of thaw subsidence and frost heave, misalignment between products from different geometries can indicate that errors are affecting the specific seasonal products. As the observation window varies from one year to another, the length of the time series also varies. We preserved the longest possible time series while ensuring that snow cover and other decorrelation factors did not affect the data quality.

The interannual time series are combining several years (2018–2024). The snow periods remain undocumented (data gaps) but one-year interferograms were used to connect the snow-free seasons. The interannual time series complement the seasonal datasets by capturing long-term displacement trends in areas where coherence can be maintained between consecutive snow-free periods. Small seasonal changes may remain due to interannual climatic variability, but these products are not intended to document seasonal patterns.

The interannual products are generally noisier than the seasonal ones, due to the impact of various sources of surface changes that can impact the signal quality when considering long time intervals (from one year to the next). Interpretation should therefore focus on relative long-term trends rather than short-term or isolated displacement patterns (**Figure 20**). Polygon averaging is again recommended to reduce the noise level and comparison between the two geometries can provide an indication on the level of consistency and uncertainty.

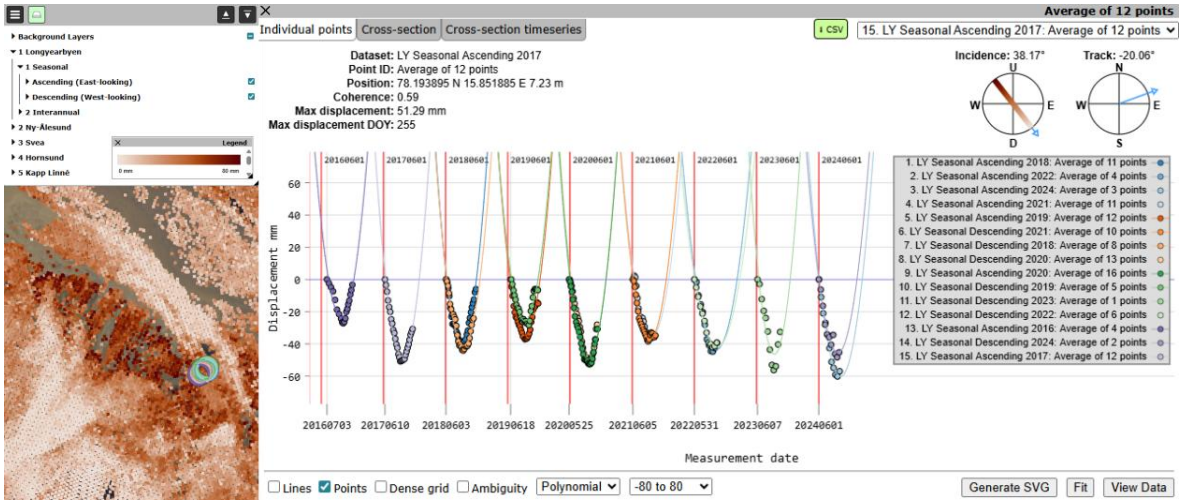

Figure 19. Comparison between several seasons and geometries. Example displaying all seasonal time series together in an ice-rich area in Adventdalen depicting thaw subsidence and frost heave cyclic patterns. When analysing the results, one should always remember that the years are not connected. They were processed independently and therefore always starts at zero. The observation time window varies from a year to another. Background: Svalbard Orthophoto (NPI, 2026b).

6. References

AMAP: AMAP Arctic Climate Change Update 2021: Key Trends and Impacts, Arctic Monitoring and Assessment Programme (AMAP), Tromsø, Norway, viii+148pp, ISBN 978-82-7971-201-5, www.amap.no/documents/doc/amap-arctic-climate-change-update-2021-key-trends-and-impacts/3594, 2021.

Antonova, S., Duguay, C. R., Kääb, A., Heim, B., Langer, M., Westermann, S., and Boike, J.: Monitoring bedfast ice and ice phenology in lakes of the Lena river delta using TerraSAR-X backscatter and coherence time series, Remote Sens., 8(11), 903, doi.org/10.3390/rs8110903, 2016.

Bamler, R., and Hartl, P.: Synthetic Aperture Radar Interferometry, Inverse Probl., 14(4), R1, doi.org/10.1088/0266-5611/14/4/001, 1998.

Barboux, C., Delaloye, R., and Lambiel, C.: Inventorying slope movements in an Alpine environment using DInSAR, Earth Surf. Process. Landf., 39(15), 2087–2099, doi.org/10.1002/esp.3603, 2014.

Berardino, P., Fornaro, G., Lanari, R., and Sansosti, E.: A new algorithm for surface deformation monitoring based on small baseline differential SAR interferograms, IEEE Trans. Geosci. Remote Sens., 40(11), 2375–2383, doi.org/10.1109/TGRS.2002.803792, 2002.

Biskaborn, B. K., Smith, S. L., Noetzli, J., Matthes, H., Vieira, G., Streletskiy, D. A., ... and Lantuit, H.: Permafrost is warming at a global scale, Nat. Commun., 10(1), 264, doi.org/10.1038/s41467-018-08240-4, 2019.

Bredal, M., Rouyet, L., Wendt, L., Hindberg, L., Stødle, D., Lauknes, T. R., Aslan, G., Hauglin, E., Dehls, J., Sundal, A., and Moldestad, D. A.: InSAR Svalbard Ground Motion Service: Observing Surface Displacements in the High Arctic, Zenodo [data set], doi.org/10.5281/zenodo.18442696, 2026.

Cai, J., Liu, G., Jia, H., Zhang, B., Wu, R., Fu, Y., ... and Zhang, R.: A new algorithm for landslide dynamic monitoring with high temporal resolution by Kalman filter integration of multiplatform time-series InSAR processing, Int. J. Appl. Earth Obs. Geoinf., 110, 102812, doi.org/10.1016/j.jag.2022.102812, 2022.

Chen, C. W., and Zebker, H. A.: Phase unwrapping for large SAR interferograms: Statistical segmentation and generalized network models, IEEE Trans. Geosci. Remote Sens., 40(8), 1709–1719, doi.org/10.1109/TGRS.2002.802453, 2002.

Costantini, M., Minati, F., Trillo, F., Ferretti, A., Novali, F., Passera, E., ... and Andersen, H. S.: European Ground Motion Service (EGMS), in: Proceedings of the 2021 IEEE International Geoscience and Remote Sensing Symposium IGARSS, Brussels, Belgium, 11–16 July 2021, 3293–3296, doi.org/10.1109/IGARSS47720.2021.9553562, 2021.

Daout, S., Doin, M. P., Peltzer, G., Socquet, A., and Lasserre, C.: Large-scale InSAR monitoring of permafrost freeze-thaw cycles on the Tibetan Plateau, Geophys. Res. Lett., 44(2), 901–909, doi.org/10.1002/2016GL070781, 2017.

Dehls, J. F., Larsen, Y., Marinkovic, P., Lauknes, T. R., Stødle, D., and Moldestad, D. A.: INSAR.No: A National InSAR Deformation Mapping/Monitoring Service in Norway--From Concept to Operations, in: Proceedings of the 2019 IEEE International Geoscience and Remote Sensing Symposium, Yokohama, Japan, 28 July 2019 – 02 August 2019, 5461–5464, doi.org/10.1109/IGARSS.2019.8898614, 2019.

Duchossois, G., Strobl, P., Toumazou, V., Antunes, S., Bartsch, A., Diehl, T., Dinessen, F., … and de Witte, E.: User Requirements for a Copernicus Polar Mission - Phase 2 Report, EUR 29144 EN, Publications Office of the European Union, Luxembourg, ISBN 978-92-79-80960-6, JRC111068, doi.org/10.2760/44170, 2018.

Duchossois, G., Berdahl, M., Diehl, T., Garric, G., Humbert, A., Itkin, P., Jawak, S., and Tietsche, S.: Copernicus Polar Roadmap for Service Evolution, Publications Office of the European Union, Luxembourg, doi.org/10.2889/644108, 2024.

Emardson, T. R., Simons, M., and Webb, F. H.: Neutral atmospheric delay in interferometric synthetic aperture radar applications: Statistical description and mitigation, J. Geophys. Res. Solid Earth, 108(B5), doi.org/10.1029/2002JB001781, 2003.

Ferretti, A.: Satellite InSAR Data: Reservoir Monitoring from Space (Vol. EET 9), EAGE European Association of Geoscientists and Engineers, doi.org/10.3997/9789462820036, 2014.

Geudtner, D., Torres, R., Snoeij, P., Davidson, M., and Rommen, B.: Sentinel-1 system capabilities and applications, in: Proceedings of the 2014 IEEE Geoscience and Remote Sensing Symposium, Quebec City, QC, Canada, 13–18 July 2014, 1457–1460, doi.org/10.1109/IGARSS.2014.6946711, 2014.

Granberg, M. E., Ask, A., and Gabrielsen, G. W.: Local contamination in Svalbard: Overview and suggestions for remediation actions, Report No. 044, Norwegian Polar Institute, ISBN 978-82-7666-408-9, hdl.handle.net/11250/2456307, 2017.

Hanssen, R. F.:. Radar Interferometry: Data Interpretation and Error Analysis (Vol. 2), Springer Science & Business Media, doi.org/10.1007/0-306-47633-9, 2001.

Hanssen-Bauer, I., Førland, E. J., Hisdal, H., Mayer, S., Sandø, A. B., and Sorteberg, A.: Climate in Svalbard 2100 - a knowledge base for climate adaptation. Chapter 7. Permafrost, avalanches and landslides, NCCS report no. 1/2019, Norwegian Centre for Climate Services, ISSN 2387-3027, hdl.handle.net/10037/18819, 2019.

Harris, C., Kern-Luetschg, M., Christiansen, H. H., and Smith, F.: The role of interannual climate variability in controlling solifluction processes, Endalen, Svalbard, Permafr. Periglac. Process., 22(3), 239–253, doi.org/10.1002/ppp.727, 2011.

Hjort, J., Streletskiy, D., Doré, G., Wu, Q., Bjella, K., and Luoto, M.: Impacts of permafrost degradation on infrastructure, Nat. Rev. Earth Environ., 3(1), 24–38, doi.org/10.1038/s43017-021-00247-8, 2022.

Larsen, Y., Engen, G., Lauknes, T. R., Malnes, E., and Høgda, K. A.: A generic differential interferometric SAR processing system, with applications to land subsidence and snow-water equivalent retrieval, in: Proceedings of the Fringe 2005 Workshop, Frascati, Italy, 28 Nov. – 2 Dec. 2005, ESA SP-610, adsabs.harvard.edu/full/2006ESASP.610E..56L, 2006.

Lauknes, T. R., Zebker, H. A., and Larsen, Y.: InSAR deformation time series using an L1-norm small-baseline approach, IEEE Trans. Geosci. Remote Sens., 49(1), 536–546, doi.org/10.1109/TGRS.2010.2051951, 2010.

Liu, L., Schaefer, K. M., Chen, A. C., Gusmeroli, A., Zebker, H. A., and Zhang, T.: Remote sensing measurements of thermokarst subsidence using InSAR, J. Geophys. Res. Earth Surf., 120(9), 1935–1948, doi.org/10.1002/2015JF003599, 2015.

Massonnet, D., and Feigl, K. L.: Radar interferometry and its application to change in the Earth's surface, Rev. Geophys., 36(4), 441–500. doi.org/10.1029/97RG03139, 1998.

Michaelides, R. J., Schaefer, K., Zebker, H. A., Parsekian, A., Liu, L., Chen, J., Natali, S., Ludwig, S. and Schaefer, S. R.: Inference of the impact of wildfire on permafrost and active layer thickness in a discontinuous permafrost region using the remotely sensed active layer thickness (ReSALT) algorithm, Environ. Res. Lett., 14(3), 035007, doi.org/10.1088/1748-9326/aaf932, 2019.

Middleton, A.: Norwegian and Russian settlements on Svalbard: An analysis of demographic and socio-economic trends, Polar Rec., 59, e14, doi.org/10.1017/S0032247423000050, 2023.

NGU: About InSAR Norge – Map of subsidence and unstable rock formations, Geological Survey of Norway (NGU), ngu.no/en/geological-mapping/about-insar-norge-map-subsidence-and-unstable-rock-formations, 2026.

Nicu, I. C., Guzman, P., and Stoleriu, C. C.: Unfreezing the past: near Pan-Svalbard assessment of cryospheric hazards to Arctic cultural heritage, Sci. Total Environ., 1000, 180424, doi.org/10.1016/j.scitotenv.2025.180424, 2025.

Nicu, I. C., Rouyet, L., Rubensdotter, L., Sinitsyn, A., Wendt, L., Christiansen, H. H., and Loktu, L.: Permafrost-related hazard, vulnerability and risk estimates for cultural heritage and modern buildings in Svalbard [Data set]. Zenodo. doi.org/10.5281/zenodo.18154592, 2026.

NPI: Terrengmodell Svalbard (S0 Terrengmodell), Norwegian Polar Institute (NPI) [data set], doi.org/10.21334/NPOLAR.2014.DCE53A47, 2014.

NPI: NP Basiskart Svalbard WMTS. Basemap service – Svalbard Topography, Norwegian Polar Institute (NPI), geodata.npolar.no, 2026a.

NPI: NP Ortofoto Svalbard WMTS. Basemap service – Svalbard Orthophoto. Norwegian Polar Institute (NPI), geodata.npolar.no, 2026b.

O'Neill et al., 2023 O'Neill, H. B., Smith, S. L., Burn, C. R., Duchesne, C., and Zhang, Y.: Widespread permafrost degradation and thaw subsidence in northwest Canada, J. Geophys. Res. Earth Surf., 128(8), e2023JF007262, doi.org/10.1029/2023JF007262, 2023.

Rantanen, M., Karpechko, A. Y., Lipponen, A., Nordling, K., Hyvärinen, O., Ruosteenoja, K., ... and Laaksonen, A.: The Arctic has warmed nearly four times faster than the globe since 1979, Commun. Earth Environ., 3(1), 168, doi.org/10.1038/s43247-022-00498-3, 2022.

Rosen, P. A., Hensley, S., Joughin, I. R., Li, F. K., Madsen, S. N., Rodriguez, E., and Goldstein, R. M.: Synthetic aperture radar interferometry. Proc. IEEE, 88(3), 333–382, doi.org/10.1109/5.838084, 2002.

Rouyet, L., Eckerstorfer, M., Lauknes, T. R., and Riise, T.: Deformasjonskartlegging rundt Longyearbyen ved bruk av satellittbasert radar interferometri, Norut rapport 13/2017, Norut Northern Research Institute, ISBN 978-82-7492-359-1, hdl.handle.net/11250/2647824, 2017.

Rouyet, L., Lauknes, T. R., Christiansen, H. H., Strand, S. M., and Larsen, Y.: Seasonal dynamics of a permafrost landscape, Adventdalen, Svalbard, investigated by InSAR, Remote Sens. Environ., 231, 111236, doi.org/10.1016/j.rse.2019.111236, 2019.

Rouyet, L., Liu, L., Strand, S. M., Christiansen, H. H., Lauknes, T. R., and Larsen, Y.: Seasonal InSAR displacements documenting the active layer freeze and thaw progression in central-western Spitsbergen, Svalbard, Remote Sens., 13(15), 2977, doi.org/10.3390/rs13152977, 2021a.

Rouyet, L., Lilleøren, K. S., Böhme, M., Vick, L. M., Delaloye, R., Etzelmüller, B., Lauknes, T. R., Larsen, Y. and Blikra, L. H.: Regional morpho-kinematic inventory of slope movements in northern Norway, Front. Earth Sci., 9, 681088, doi.org/10.3389/feart.2021.681088, 2021b.

Rouyet, L., Bredal, M., Lauknes, T.R., Dehls, J., Larsen, Y., van Oostveen, J., Hindberg, H., and Wendt, L.: InSAR Svalbard – User requirement, technical considerations, and product development plan, Report 2-2024-NORCE-Energy and Technology, NORCE Research AS, ISBN 978-82-8408-341-4, hdl.handle.net/11250/3125660, 2024.

Rudy, A. C., Lamoureux, S. F., Treitz, P., Short, N., and Brisco, B.: Seasonal and multi-year surface displacements measured by DInSAR in a High Arctic permafrost environment, Int. J. Appl. Earth Obs. Geoinf., 64, 51–61, doi.org/10.1016/j.jag.2017.09.002, 2018.

Samsonov, S. V., Lantz, T. C., Kokelj, S. V., and Zhang, Y.: Growth of a young pingo in the Canadian Arctic observed by RADARSAT-2 interferometric satellite radar, The Cryosphere, 10(2), 799–810, doi.org/10.5194/tc-10-799-2016, 2016.

Strand, S. M., and Christiansen, H. H.: Permafrost thermal regime and active layer dynamics across periglacial landforms in Svalbard's Nordenskiöld Land Permafrost Observatory, 2008–2023, Arctic Sci., 11, 1–19, doi.org/10.1139/as-2024-0027, 2025.

Streletskiy, D. A., Maslakov, A., Grosse, G., Shiklomanov, N. I., Farquharson, L., Zwieback, S., ... and Debolskiy, M. V.: Thawing permafrost is subsiding in the Northern Hemisphere—review and perspectives, Environ. Res. Lett., 20(1), 013006, doi.org/10.1088/1748-9326/ada2ff, 2025.

Strozzi, T., Antonova, S., Günther, F., Mätzler, E., Vieira, G., Wegmüller, U., ... and Bartsch, A.: Sentinel-1 SAR interferometry for surface deformation monitoring in low-land permafrost areas, Remote Sens., 10(9), 1360, doi.org/10.3390/rs10091360, 2018.

Swanson, D. K.: Permafrost thaw-related slope failures in Alaska's Arctic National Parks, c. 1980–2019, Permafr. Periglac. Process., 32(3), 392-406, doi.org/10.1002/ppp.2098, 2021.

Wang, L., Marzahn, P., Bernier, M., and Ludwig, R.: Sentinel-1 InSAR measurements of deformation over discontinuous permafrost terrain, Northern Quebec, Canada, Remote Sens. Environ., 248, 111965, doi.org/10.1016/j.rse.2020.111965, 2020.

Wendt, L., Rouyet, L., Christiansen, H. H., Lauknes, T. R., and Westermann, S.: InSAR sensitivity to active layer ground ice content in Adventdalen, Svalbard, The Cryosphere, 20, 1179–1197, doi.org/10.5194/tc-20-1179-2026, 2026.

Woodhouse, I. H.:. Introduction to Microwave Remote Sensing. CRC press, doi.org/10.1201/9781315272573, 2006

Zwieback, S., and Hajnsek, I.: The impact of vegetation growth on DInSAR coherence regions and estimated deformations, in: Proceedings of the 2014 IEEE Geoscience and Remote Sensing Symposium, Quebec City, QC, Canada, 13–18 July 2014, 966–969. doi.org/10.1109/IGARSS.2014.6946587, 2014.

Zwieback, S., Hensley, S., and Hajnsek, I.: Assessment of soil moisture effects on L-band radar interferometry, Remote Sens. Environ., 164, 77–89, doi.org/10.1016/j.rse.2015.04.012, 2015.

Zwieback, S., and Meyer, F. J.: Top-of-permafrost ground ice indicated by remotely sensed late-season subsidence, Cryosphere, 15(4), 2041–2055, doi.org/10.5194/tc-15-2041-2021, 2021.

Zwieback, S., Liu, L., Rouyet, L., Short, N., and Strozzi, T.: Advances in InSAR analysis of permafrost terrain, Permafr. Periglac. Process., 35(4), 544–556, doi.org/10.1002/ppp.2248, 2024.